Acp-2016-584-revision

Comments (in *italics*), responses, and marked-up revised manuscript

General Comments from Anonymous referee # 1

This manuscript is a very solid description of aerosols from a unique and understudied region (Antarctic). The study provides unique and valuable data regarding two samples (summer and winter) that have distinct differences in their composition. The combination of the three methods, particularly the Raman/ATR-FTIR comparison, is a powerful unified approach to explore the detailed physicochemical composition of these particles. The Ro group has really advanced the ATR-FTIR coupled with Raman approach that allows for insights regarding how sulfate is bound, for example. Overall, the data interpretation is thorough and solid. The authors do a nice job of placing their results in the context of other research in the field. A few small issues should be addressed in a revised manuscript and are indicated below. Overall, this manuscript has the potential to be a useful contribution to the field.

Response: We thank the reviewer for his/her positive evaluation of our work and valuable comments.

Major comments from Anonymous referee #1

One major concern with the manuscript is the drawing of broad conclusions with limited samples. Specifically, connecting everything back to the biological content without knowledge of sample to sample variability during the different seasons. Given the samples collected this might not be possible, but some discussion of the degree of variability that would occur between two samples of the same season would help provide context as to how much these differences are due to real differences between seasons or differences that happen to occur between these two specific samples that could be due to other reasons.

Response: The reviewer is right in terms that it is unclear whether the different compositional features between two samples are due to their different sampling seasons or biological activities. To answer this question, a study for overall 29 Antarctic aerosol samples is underway. We hope that this further study can provide us better understanding about the Antarctic SSAs. In the revised manuscript, we mentioned this point by modifying a paragraph ("First, although just two SSA samples, having a high chlorophyll-*a* level contrast, collected in the summer and winter were investigated, their chemical compositional features were clearly different in terms of their chemical species and/or levels of inorganic and organic moieties. However, it is not clear whether the different compositional features are due to their different sampling seasons or biological activities. To answer this question, a study for overall 29 Antarctic aerosol samples collected during Dec. 2011 and Sep. 2012 when the oceanic chlorophyll-*a* levels were in the range of 0.07-13.38 μg/L is underway." – p. 18, lines 528-535 in the revised manuscript).

The second concern is that, while the authors do go to great lengths to justify it, I remain not fully convinced that the organic spectra can be so definitively identified as alanine. Additionally, the confidence of assigning it to the Mg-hydrate salt seems not fully justified, given the challenge of distinguishing ions such as Ca^{2+} from Mg^{2+} in ambient vibrational spectra. I believe that alanine is likely one of a number of compounds contributing to the modes observed, along with the associated hydrate salts of different cations. The authors should soften that language a little to make clear that alanine is unlikely to be the sole contributor to those modes. The classification for fatty acids by contrast appears to be the appropriate level of specificity.

      Response: We admit that Raman and ATR-FTIR spectra of MgAla-containing Antarctic SSAs do not perfectly match with those of aerosols nebulized from standard alanine and MgCl2 mixture solutions. Therefore, MgAla-containing SSAs should be mainly composed of MgAla with the very small amounts of other unknown components. It is also true that sometimes Ca salts cannot be easily distinguished from Mg salts, and yet most Ca ions are combined with sulfate according to X-ray and Raman mapping results, excluding the consideration of Ca salts in the assignment. We carefully rewrote the revised manuscript not to convey the impression that MgAla-containing SSAs are solely composed of MgAla. Regarding this comment, some modification is

given in the revised manuscript ("the frequently observed organic species are most probably ones containing Mg hydrate salts of alanine (MgAla) and Mg salts of fatty acids (MgFAs)." – p. 11, lines 304-305; "Divalent Ca ions are also present in sea-water. However, based on X-ray and Raman mapping results, Ca ions are mostly combined with inorganic SO_4^{2-} and slightly present in regions where organic moieties are. Based on a comparison of the Raman and ATR-FTIR spectra obtained for the summertime SSAs and aerosols generated from the mixture solution of standard alanine and $MgCl_2$, the organic species are ones containing mainly the Mg hydrate salts of alanine (MgAla), even though their precise molecular formula and the other possible minor components could not be confirmed." – p.12, lines 353-360; "it is clear that MgAla-containing SSAs are composed of mainly alanine with negligible glycine and other target chemicals." – p.13, line 383-384) together with tone-downed wording.

There is very little discussion of the nitrate observed in the samples, particularly in the sample S2. Given the distinctly different HYSPLITs between samples 1 and 2 the enrichment of NO_3^- in S2 that passes over Chile seems to provide evidence of heterogeneous processing through the classic NaCl + HNO₃ → HCl + NaNO₃ reaction. This is barely discussed, but seems like an important point that should be discussed in more detail. Aging of SSA and organics from SSA is well established with EDX and Raman [Adachi and Buseck, 2015; Ault et al., 2013; Ault et al., 2014; Laskin et al., 2012; Liu et al., 2011; Trueblood et al.,2016], but primarily from CAICE-style waveflume experiments or in field studies the mid-latitudes. Discussion of heterogeneous aging in the less-studied Antarctic in the context of the impact observed and modeled [Bauer et al., 2007] in the midlatitudes would strengthen the impact of the paper.

Response: NO3- is more frequently observed in sample S1 than in sample S2 (see Table 2), suggesting nitrates of a marine origin rather than of an anthropogenic origin from Chile. To discuss the observation of nitrates, we insert a paragraph ("Although N X-ray signal was not detected probably due to the small amount of NO_3^- present in the Antarctic SSAs, $Mg(NO_3)_2$ and $NaNO_3$ were frequently observed in samples S1 and S2 using Raman and ATR-FTIR techniques. The nitrate in sea-water can be generated by the photoammonification process, which transforms dissolved organic nitrogen (DON) to labile inorganic nitrogen, mainly ammonium (NH_4^+) (Kitidis

et al., 2006; Aarnos et al., 2012; Xie et al., 2012; Rain-Franco et al., 2014; Paulot et al., 2015), followed by the microbial oxidation of ammonium into nitrate (NO_3^-) by nitrifying bacteria (Carlucci et al., 1970; Hovanec and Delong, 1996; Smith et al., 2014; Tolar et al., 2016). As the photoammonification depends on solar radiations, the ammonium and nitrate production would be enhanced in the summer with higher solar radiation level. Indeed, as shown in Table 2, nitrates are more frequently observed in summertime sample S1 than wintertime sample S2." – p. 15, lines 439-449).

Minor comments from Anonymous referee #1

This is a stylistic point, but I believe the "a" in "Chlorophyll-a" should be italicized.

Response: Corrected in revised text. We thank the reviewer for pointing out the error.

The uncertainty of the chl-a measurements should be discussed further. Specifically, what is the LOD? The uncertainty should be included when referenced in the abstract and experimental sections in the form of +/- after the values. How certain are the authors that the difference is really 19 time for summer versus winter. This should be addressed further.

Response: We did not clearly state that the *chl-a* levels are for the nearby oceanic water collected on the sampling days of the samples, which are not mean *chl-a* levels for the summer and winter. In the revised manuscript, we made this point clear and provided the description of *chl-a* determination and references ("This study examined two aerosol samples S1 and S2 collected on Dec. 9, 2011 in the austral summer and July 23, 2012 in the austral winter, respectively, when the oceanic chlorophyll-*a* levels on the collection days of the samples were quite different, by ~19 times (2.46 vs. 0.13 μg/L, respectively). The oceanic chlorophyll-*a* levels for water samples collected daily from nearby oceanic water were determined using a fluorometer (TD 700, Turner Design, USA)). The detailed description for chlorophyll-*a* determination is given elsewhere (Schloss et al., 2014; Lee et al., 2015)." – p. 4, lines 93-99).

On lines 74-75 it could be interpreted that two samples were collected total or that 2 samples from summer and 2 from winter were collected. Consider revising to make this clear.

Response: Corrected ("two Antarctic aerosol samples collected on Dec. 9, 2011 in the austral summer (sample S1) and July 23, 2012 in the austral winter (sample S2)" p. 3, lines 75-77).

Lines 102-107 As noted above, some further comparison of the differences between the Hysplit trajectories would be useful for data interpretation.

Response: Please refer to our response above.

Further discussion of the organic overlay from Raman and with elemental overlay from EDX would be useful. It seems that the organic portions from the Raman are the thickest portions. This is not necessarily intuitive, though the 2800-3000 window seems like a logical choice.

Response: Further discussion is given in the revised manuscript **("**Molecular Raman images look broader than elemental X-ray images as the spatial resolution of Raman mapping (~1 μm) is larger than that of X-ray mapping (~0.1 μm). Especially, Raman images for organic species look more spread than C X-ray map images as the low energy C X-rays generated from underneath are not often detected due to the strong absorption by solid particles sitting above." – p. 7, lines 198-202).

The silicon-containing particles are interesting. Why would the enhanced sea ice noted on lines 264-265 specifically hinder Si species emission? Is there something about the winter time emissions that is somehow chemically selective? This was unclear and should be explained in more detail.

Response: Production of silicone component can be related to diatom activities, which would be higher in the summer. As the effect of sea ice cap is not clear, the ice cap thing is removed in the

revised manuscript ("In the winter, the reduced diatom activities would decrease the emission of Si species into the atmosphere, resulting in the scarce observation of Si in the S2 sample." – p. 8, lines 274-275).

For the 1052 cm^{-1} peak noted on line 300, how are the authors able to distinguish Mg(NO$_3$)$_2$ the symmetric stretch of the aqueous nitrate ion observed around 1055 cm^{-1}? See [Zangmeister and Pemberton, 2001]and [Ault et al., 2014] for reference. It seems unlikely that the two peaks could be distinguished cleanly and that even if one is present there may be contribution from the other mode.

Response: As Raman spectra show no free water in the SSAs and SEIs indicate solid SSAs, we think that the presence of aqueous nitrate is ignorable.

The phrase "encountering frequency" is used frequently, but is an odd choice of wording. It is suggested that it be replaced with different terminology, as well as to clearly define the terminology used.

Response: We agree with the reviewer's comment. In the revised manuscript, "encountered" is mostly replaced by "observed". The definition of "encountering frequency" is given in the revised manuscript ("where the relative encountering frequency (in %) for a certain element is defined as the number of particles containing the element divided by the total number of particles analyzed for a sample" – p. 6, lines 176-178).

General Comments from Anonymous referee # 2

This is an interesting paper that focuses on the integration of several single particle techniques to investigate sea spray aerosol samples collected at King Sejong Korean scientific research station in the austral summer and in the austral winter. Through use of these single particle techniques several conclusions are drawn related to the identification of organic compounds and inorganic

salts. Some of the observations reported in the paper have been seen before and confirm earlier studies (e.g. chloride depletion in particles).

Response: We thank the reviewer for the positive evaluation of our work.

Specific comments from Anonymous referee # 2

In many particles, there is nitrate observed in the particles - where does the nitrate come from in these particles?

Response: We provided discussion in the revised manuscript as follows; "Although N X-ray signal was not detected probably due to the small amount of NO_3^- present in the Antarctic SSAs, $Mg(NO_3)_2$ and $NaNO_3$ were frequently observed in samples S1 and S2 using Raman and ATR-FTIR techniques. The nitrate in sea-water can be generated by the photoammonification process, which transforms dissolved organic nitrogen (DON) to labile inorganic nitrogen, mainly ammonium (NH_4^+) (Kitidis et al., 2006; Aarnos et al., 2012; Xie et al., 2012; Rain-Franco et al., 2014; Paulot et al., 2015), followed by the microbial oxidation of ammonium into nitrate (NO_3^-) by nitrifying bacteria (Carlucci et al., 1970; Hovanec and Delong, 1996; Smith et al., 2014; Tolar et al., 2016). As the photoammonification depends on solar radiations, the ammonium and nitrate production would be enhanced in the summer with higher solar radiation level. Indeed, as shown in Table 2, nitrates are more frequently observed in summertime sample S1 than wintertime sample S2." – p. 15, lines 439-449.

Why is alanine such a dominant factor in the SSA? Are there other compounds that can have similar spectral features? It seems too simple to have one compound and one complex Mg-alanine in sea spray particles. The case for fatty acids seems more convincing given several studies that have identified palmitate and stearate in sea spray aerosol.

Response: The reviewer #1 also made the same comment. Please refer to our response to the comment by the reviewer #1.

Some of the figure captions in the supplemental do not match or explain well the figure making it difficult to understand what is being shown. (See for example Figure S3 – what are the three sets of spectra shown?)

Response: Figure captions in the supplement are modified as below.

Figure S3. Raman and ATR-FTIR spectra of the aerosols generated by the nebulization of a mixture solution of 0.2 M alanine and 0.1 M $MgCl_2$ standard chemicals. The first pair of Raman and ATR-FTIR spectra for the aerosols was obtained just after the nebulization and the second and third pairs of Raman and ATR-FTIR spectra were obtained ~1 year later after the storage in a desiccator. The first and third pairs of Raman and ATR-FTIR spectra for organic moiety look similar to those in Figures 4(b) and 4(a), respectively

Figure S4. Raman and ATR-FTIR spectra of some target chemicals for organics in Antarctic SSAs, which do not resemble with those for MgAla-containing SSAs.

Figure S5. Raman and ATR-FTIR spectra of powdery standard Mg palmitate, palmitic acid, Mg stearate, and stearic acid, which are sufficiently different to distinguish the four compounds

Figure S6. ATR-FTIR spectra of Mg palmitate, Mg stearate, a mixture of Mg palmitate and stearate (by 3:1), and MgFAs-containing SSA, showing that MgFAs-containing SSAs are the mixture of mainly Mg palmitate and stearate.

Figure S7. Raman and ATR-FTIR spectra of standard inorganic chemicals, which are observed in Antarctic SSAs.

1 **Single-particle investigation of summertime and wintertime Antarctic sea spray aerosols**

2 **using low-*Z* particle EPMA, Raman microspectrometry, and ATR-FTIR imaging**

3 **techniques**

4

5 Hyo-Jin Eom[1], Dhrubajyoti Gupta[1], Hye-Rin Cho[1], HeeJin Hwang[2], SoonDo Hur[2], Yeontae

6 Gim[3] and Chul-Un Ro[1,*]

7

8 [1]*Department of Chemistry, Inha University, Incheon, Republic of Korea*

9 [2]*Polar Climate Change Research Division, Korea Polar Research Institute, Incheon, Republic of*

10 *Korea*

11 [3]*Arctic Research Center, Korea Polar Research Institute, Incheon, Republic of Korea*

12

13 **ABSTRACT**

14   Two aerosol samples collected at King Sejong Korean scientific research station,

15 Antarctica on Dec. 9, 2011 in the austral summer (sample S1) and July 23, 2012 in the austral

16 winter (sample S2), when the oceanic chlorophyll-*a* levels on the collection days of the samples

17 were quite different, by ~19 times (2.46 vs. 0.13 μg/L, respectively), were investigated on a single

18 particle basis using quantitative energy-dispersive electron probe X-ray microanalysis (ED-

19 EPMA), called low-*Z* particle EPMA, Raman microspectrometry (RMS), and attenuated total

20 reflectance Fourier transform infrared (ATR-FTIR) imaging techniques to obtain their

21 characteristics based on the elemental chemical compositions, molecular species, and mixing state.

22 X-ray analysis showed that the supermicron summertime and wintertime Antarctic aerosol samples

23 have different elemental chemical compositions, even though all the individual particles analyzed

24 were sea spray aerosols (SSAs); i.e., the contents of C, O, Ca, S, and Si were more elevated,

25 whereas Cl was more depleted, for sample S1 than for sample S2. Based on qualitative analysis of

26 the chemical species present in individual SSAs by the combined application of RMS and ATR-

27 FTIR imaging, different organic species were observed in samples S1 and S2; i.e., Mg hydrate

28 salts of alanine were predominant in samples S1 and S2, whereas Mg salts of fatty acids internally

*Corresponding author. Tel.: +82 32 860 7676; fax: +82 32 874 9207

E-mail address: curo@inha.ac.kr (C.-U. Ro)

29 mixed with Mg hydrate salts of alanine were significant in sample S2. Although $CaSO_4$ was

30 observed significantly in both samples S1 and S2, other inorganic species, such as Na_2SO_4, $NaNO_3$,

31 $Mg(NO_3)_2$, SiO_2, and CH_3SO_3Mg, were observed more significantly in sample S1, suggesting that

32 those compounds may be related to the higher phytoplankton activity in summer.

33

34 **INTRODUCTION**

35   As more than 70% of the Earth's surface is covered by ocean, sea spray aerosols (SSAs)

36 make a dominant contribution to the total aerosol load in the air (Quinn et al., 2015). The influence

37 of nascent SSAs on the Earth′s radiative balance, either directly by scattering light or indirectly by

38 acting as cloud droplets or ice nuclei, needs to be understood to better predict the additional

39 anthropogenic effects on SSAs (Ault et al., 2013a). Recently, it was suggested that SSAs mixed

40 with organic matter occurring at the ocean surface can have a significant influence on the Earth's

41 climate change (Wang et al., 2015). In addition, an understanding of the nascent SSA properties in

42 terms of the physical, chemical, and biological processes in the ocean surface is required to reduce

43 the current uncertainties for climate models (Prather et al., 2013).

44   SSAs are generated by bubbles bursting at the sea surface, where submicron and

45 supermicron SSAs are believed to be formed mostly from film drops and jet drops, respectively

46 (Quinn et al., 2014; Quinn et al., 2015; Wang et al., 2015). Submicron nascent SSAs were reported

47 to have more enriched organic species and less inorganic salts than the supermicron nascent SSAs

48 (Ault et al., 2013b; Prather et al., 2013; Wang et al., 2015). Although the molecular species of the

49 organic matter in nascent SSAs are unknown, a recent mesocosm experiment showed that

50 submicron SSAs were enriched with aliphatic-rich organic species, whereas supermicron SSAs

51 contained more oxidized organic species (Wang et al., 2015). As organic and inorganic matter in

52 sea water could be produced through the biological food web, the chemical compositions in

53 nascent SSAs would be interrelated with the biological activity in sea-water. On the other hand,

54 there have been disputes regarding the correlation between the biological activity in the ocean and

55 SSA organic matter in the marine boundary layer. Some studies reported positive correlations

56 between the levels of chlorophyll-*a*, which is an indicator of the biological activity in the sea-water,

57 and organic matter in SSAs (Prather et al., 2013; Hu et al., 2013; Rinaldi et al., 2010; O'Dowd et

58 al., 2004), whereas some showed no correlation between them (Quinn et al., 2014; Bates et al.,

59 2012). In addition, it was claimed that the chlorophyll-*a* level showed a complicated correlation
60 with the organic matters in nascent SSAs and the bacterial enzyme activities should also be
61 considered to better understand the overall generation and temporal variations of organic matter
62 (Wang et al., 2015), strongly suggesting the necessity for further studies.

63   The Antarctic region, which is isolated from anthropogenic sources, is one of the few
64 pristine places to study natural SSAs with a minimal anthropogenic influence (Maskey et al., 2011).
65 A major constituent in the Antarctic troposphere is nascent SSAs (Hara et al., 2012; Maskey et al.,
66 2011) and their chemical compositions can be altered through heterogeneous reactions with SO_4^{2-}
67 and $CH_3SO_3^-$ during the summer (Hara et al., 2014). Some studies on the characterization and
68 seasonal cycles of different aerosol species at various Antarctic locations, such as McMurdo (Ross
69 Island), Aboa (Queen Maud Land), Syowa (East Ongul Island), Dome Fuji (Queen Maud Land),
70 O'Higgins (Chile), Admiralty Bay (King George Island), and Mizuho (Atka Bay) stations, have
71 been carried out, and bulk and single-particle analytical techniques showed that the sea-salts and
72 sulfur-containing species were the most abundant constituents in Antarctic aerosol samples (Hara
73 et al., 2013; Hara et al., 2012; Maskey et al., 2011; Préndez et al., 2009; Biancato et al., 2006;
74 Hara et al., 2006; Kerminen et al., 2000; Shaw, 1988). In this study, two Antarctic aerosol samples
75 collected on Dec. 9, 2011 in the austral summer (sample S1) and July 23, 2012 in the austral winter
76 (sample S2), having a drastic contrast in the oceanic chlorophyll-*a* levels on the collection days of
77 the samples, were characterized on a single particle basis using quantitative energy-dispersive
78 electron probe X-ray microanalysis (ED-EPMA), called low-*Z* particle EPMA, Raman
79 microspectrometry (RMS), and attenuated total reflection Fourier transform infrared (ATR-FTIR)
80 imaging. In the present study, low-*Z* particle EPMA was applied to investigate the elemental
81 compositional contrast between the summertime and wintertime samples and two vibrational
82 spectroscopic techniques, such as RMS and ATR-FTIR imaging, were employed on a single
83 particle basis to identify the organic and inorganic molecular species present in Antarctic aerosol
84 samples, clearly revealing the different chemical features between two samples.
85

86 **2. EXPERIMENTAL SECTION**
87 **2.1 Samples**

88   Aerosol samples were collected at a Korean scientific research station in the Antarctic: King

89   Sejong station (62°13′S, 58°47′W), which is located at King George Island, Chile (see Figure S1

90   of the Supporting Information). King George Island in the South Ocean is 120 km off the coast of

91   Antarctica, and is dominated by pervasive ice caps, with more than 90% of the island being

92   glaciated. This study examined two aerosol samples S1 and S2 collected on Dec. 9, 2011 in the

93   austral summer and July 23, 2012 in the austral winter, respectively, when the oceanic chlorophyll-

94   a levels on the collection days of the samples were quite different, by ~19 times (2.46 vs. 0.13

95   µg/L, respectively). The oceanic chlorophyll-a levels for water samples collected daily from

96   nearby oceanic water were determined using a fluorometer (TD 700, Turner Design, USA)). The

97   detailed description for chlorophyll-a determination is given elsewhere (Schloss et al., 2014; Lee

98   et al., 2015). The aerosol samples were collected on Al foil substrates (Sigma-Aldrich, 99.8%

99   purity) using a three stage cascade impactor (PM$_{10}$ Impactor, Dekati Inc.) during daytime at

100   temperatures, T = 1.1 – 2.1 °C and -1.9 – -1.5 °C and relative humidity, RH = 94.1 – 94.5 % and

101   87.6 – 92.1 % for samples S1 and S2, respectively. The impactor had aerodynamic cut-sizes of 10,

102   2.5, and 1 µm for stages 1, 2, and 3, respectively, at a 10 L min^{-1} sampling flow, and individual

103   particles collected on stages 2 and 3 (PM$_{2.5-10}$ and PM$_{1.0-2.5}$ fractions with the size range of 2.5–10

104   µm and 1–2.5 µm, respectively) were examined.

105   Three-day (72 h) backward air-mass trajectories were obtained using the Hybrid

106   Lagrangian Single-Particle Integrated Trajectory (HYSPLIT) model from the NOAA Air

107   Resources Laboratory's web server (http://www.arl.noaa.gov/ready/hysplit4.html). The back-

108   trajectories for samples S1 and S2 show that the air-masses at heights of 500 m, 1000 m, and 1500

109   m above sea level, which originated from the Pacific Ocean, travelled over the Pacific Ocean and

110   passed over Chile, respectively (see Figure S1 of the Supporting Information).

111

112   **2.2 Low-Z particle EPMA measurement and data analysis**

113   Low-Z particle EPMA measurements were carried out by scanning electron microscopy

114   (JSM-6390, JEOL) equipped with an Oxford Link SATW ultrathin window energy-dispersive X-

115   ray (EDX) detector, which has a spectral resolution of 133 eV for Mn Kα X-rays. The X-ray spectra

116   and elemental X-ray maps were recorded using INCA Energy software. An accelerating voltage of

117   10 kV and a beam current of 0.5 nA, and a typical measuring time of 20 s were used for the X-ray

4

118 spectral data acquisition using area mode, where the X-ray signals were obtained by the scanning

119 electron beam over the entire area of each particle. The net X-ray intensities for the chemical

120 elements were obtained by a non-linear, least-square fit of the spectra collected using the AXIL

121 program (Vekemans et al., 1994). The elemental concentrations of the individual particles were

122 determined from their X-ray intensities using a Monte Carlo calculation combined with reverse

123 successive approximations (Ro et al., 2003). For the X-ray mapping measurements, an accelerating

124 voltage and beam current are the same as the area mode measurements except for a typical

125 measuring time of 30 min. A more detailed discussion of the EPMA measurement conditions can

126 be found elsewhere (Ro et al., 2005; Ro et al., 1999).

127

128 **2.3 RMS measurements**

129   The particles collected on Al foil were mounted on the microscope stage of a confocal

130 Raman microspectrometer (XploRA, Horiba Jobin Yvon) equipped with a 100×, 0.9 numerical

131 aperture objective (Olympus). Raman point and mapping measurements were carried out under

132 ambient conditions. Optical images of the particles for relocation were obtained using a video

133 camera. Raman scattering was excited at the 532 nm wavelength using an air-cooled diode laser

134 and detected with a multichannel air cooled charge-coupled device (CCD) at an 1800 gr/mm

135 grating. The excitation laser power delivered to the individual particles was approximately 3 mW

136 using a controlled confocal hole of 300 ~ 500 μm and a slit, 100 μm in diameter. The spectral

137 ranges of 100–4000 cm^{-1} were performed with a 5 s acquisition time and 5 times accumulation for

138 each measurement. The spectral resolution was 1.8 cm^{-1} and the spot size of the laser beam at the

139 sample was estimated to be ~1 μm^2. The XYZ computer-controlled Raman mapping was

140 performed by obtaining the Raman spectra in point-by-point XY scanning mode with a 1 μm step

141 and a 5 s integration time per pixel. The spectra and images were acquired using Labspec6 software.

142 A more detailed discussion of the RMS measurement conditions for single particle analysis can be

143 found elsewhere (Sobanska et al., 2012; Eom et al., 2013; Jung et al., 2014).

144

145 **2.4 ATR-FTIR imaging measurements**

146   The ATR-FTIR imaging measurements were performed using a Perkin Elmer Spectrum

147 100 FTIR spectrometer interfaced to a Spectrum Spotlight 400 FTIR microscope. An ATR

148 accessory using a germanium hemispherical IRE crystal, 600 μm in diameter, was used for ATR

149 imaging. The ATR accessory was mounted on the X–Y stage of the FTIR microscope and the IRE

150 crystal was made to come into contact with the sample through a force lever. A spatial resolution

151 of 3.1 μm at 1726 cm^{-1} ($\lambda = 5.79$ μm) is achievable (Van Dalen et al., 2007). A 16 x 1 pixel mercury

152 cadmium telluride (MCT) array detector was used to obtain the FTIR images with a pixel size of

153 1.56 μm. For each pixel, an ATR-FTIR spectrum, ranging from 680 to 4000 cm^{-1} with a spectral

154 resolution of 4 cm^{-1}, was obtained from eight interferograms, which were co-added and Fourier-

155 transformed. The position of the crystal on the sample was determined using an optical microscope

156 equipped with a light emitting diode and a CCD camera, which allowed relocation of the same

157 single particles that had been analyzed using RMS before ATR-FTIR imaging. Spectral data

158 processing was performed using Perkin Elmer Spectrum IMAGE software. A more detailed

159 discussion of the ATR-FTIR imaging measurement conditions for single particle analysis can be

160 found elsewhere (Song et al., 2010; Song et al., 2013; Jung et al., 2014).

161

162 **3. RESULTS AND DISCUSSION**

163

164 **3.1 Single-particle characterization of the summertime and wintertime Antarctic SSAs**

165 **using low-*Z* particle EPMA**

166

167 Figure 1 presents typical secondary electron images (SEIs) of the individual particles on

168 two PM$_{2.5-10}$ (stage 2) samples collected in the austral summer and winter, where the chemical

169 species comprising each particle, determined from X-ray spectral data, is indicated. All the

170 particles on the images are of a marine origin having major Na and Cl contents with small

171 quantities of C, O, Mg, K, Ca, S, and/or Si. Overall, approximately 600 particles of samples S1

172 and S2 examined by low-*Z* particle EPMA were of a marine origin. Na, Mg, Cl, S, C, and O were

173 present in all the particles, whereas K, Ca, and Si were observed more frequently in the

174 summertime sample S1 than in the wintertime sample S2 (93.6 % vs. 79.4 % relative encountering

175 frequencies for K; 93.9 % vs. 75.5 % for Ca; and 70.1 % vs. 0.7 % for Si, respectively, where the

176 relative encountering frequency (in %) for a certain element is defined as the number of particles

177 containing the element divided by the total number of particles analyzed for a sample.). In

6

178 particular, Si is present exclusively in sample S1, which might be a good indicator of the
179 phytoplankton influence on the nascent SSAs.

180   As ambient relative humidity (RH) at the sampling times were higher than 87.6% and the
181 efflorescence RHs (ERHs) of the inorganic sea salt components (e.g., ERHs of NaCl and CaSO$_4$
182 are ~45-47 % and ~80-90 %, respectively (Gupta et al., 2015; Schindelholz et al., 2014; Xiao et
183 al., 2008)), the SSAs would be collected as aqueous droplets at the time of collection. Once
184 exposed at a low RH, e.g. by being either handled under the dry ambient conditions or placed in
185 the vacuum chamber of SEM, they would crystallize fractionally, resulting in their heterogeneous
186 mixing states, as shown in Figure 1, having bright and crystalline solids, segregated and somewhat
187 dark regions, and elongated rods (indicated by the yellow arrows in Figure 1), which are more
188 distinctive for the summertime particles. The fractional crystallization of SSAs has also been
189 reported (Ault et al., 2013a; Hara et al., 2013; Hara et al., 2014). To determine the chemical species
190 of the crystalline solids, dark regions, and rods, elemental X-ray and molecular Raman mapping
191 measurements were performed on the same individual SSA particles. Figure 2 presents the SEIs
192 and molecular Raman and elemental X-ray map images of two typical summertime and wintertime
193 SSA particles. As Raman-inactive NaCl and MgCl$_2$ species cannot generate Raman signals, Raman
194 mapping was performed to determine the spatial distributions of CaSO$_4$ (using Raman signal in
195 1000 – 1020 cm^{-1} range), Na$_2$SO$_4$ (using Raman signal in 985 – 995 cm^{-1} range), and organic
196 species (using Raman signal in 2800 – 3000 cm^{-1} range). X-ray mapping images of Na, Mg, Ca,
197 Cl, S, C, and O are overlaid in different colors on the SEIs. Molecular Raman images look broader
198 than elemental X-ray images as the spatial resolution of Raman mapping (~1 μm) is larger than
199 that of X-ray mapping (~0.1 μm). Especially, Raman images for organic species look more spread
200 than C X-ray map images as the low energy C X-rays generated from underneath are not often
201 detected due to the strong absorption by solid particles sitting above. Nonetheless, the combined
202 Raman and X-ray map image data of Figure 2(a) clearly indicate that the upper bright solid (region
203 1, notated on the SEI of Figure 2(a)) of the summertime SSA particle is composed of NaCl, the
204 bottom-right region 3 is a mixture of MgCl$_2$ and organic species (having a somewhat dark
205 appearance due to the low secondary electron yield of organic species), and the two elongated rods
206 are of a mixture of CaSO$_4$ and Na$_2$SO$_4$. The wintertime SSA particle in Figure 2(b) is composed
207 of NaCl (at region 1) and the mixture of MgCl$_2$ and organic species (at region 2). As C and O are

208 overlapping in their X-ray maps of Figure 2, the organic species appear to contain a significant

209 amount of oxygen. Figure 3 shows the X-ray spectra and elemental atomic concentrations obtained

210 from the entire regions of the summertime and wintertime particles using area-mode X-ray data

211 acquisition. The summertime particle contains more C, O, Si, S, and Ca than the wintertime particle.

212 As the amount of sulfate (by assuming all the sulfur exists as sulfate) for the summertime particle

213 is larger than that of Ca, the sulfate first crystallized as $CaSO_4$, and the remaining sulfate

214 crystallized as Na_2SO_4, resulting in the formation of elongated rods composed of a mixture of

215 $CaSO_4$ and Na_2SO_4. For the wintertime particle, $CaSO_4$ was observed weakly at the upper-right

216 region because of the low sulfate content.

217 Table S1 in the Supporting Information shows the mean elemental concentrations for an

218 overall ~600 individual particles in $PM_{1.0-2.5}$ and $PM_{2.5-10}$ fractions of the summertime and

219 wintertime samples, obtained by low-Z particle EPMA. As all the particles analyzed in these

220 samples are of a marine origin, the mean atomic concentrations of Na and Cl are largest (ranging

221 in 25.2 – 28.3 % and 24.8 – 29.2 %, respectively), followed by high C and O concentrations (18.8

222 – 27.1 % and 17.3 – 19.5 %, respectively), compared to those of Mg, Si, S, K, and Ca which are

223 in the range, 0.0 – 2.9 %. Based on the mean elemental weight concentrations, the C and O contents

224 were smaller based on the mean atomic concentrations, even though they were still considerable

225 (9.6 – 14.6 % and 12.0 – 13.6 %, respectively). On the other hand, the organic contents on a

226 molecular basis would be smaller than the elemental C contents but the molecular organic content

227 could not be estimated because the organic molecular species in SSAs have not been identified

228 clearly (Ault et al., 2013b; Laskina, 2015; Quinn et al., 2015). An interesting observation was that

229 all the supermicron Antarctic SSAs both in the summertime and wintertime samples were a

230 mixture of inorganic and organic species.

231 To better examine the chemical compositional contrast between samples S1 and S2, Table

232 1 lists the mean elemental concentration ratios to Na for individual particles together with those

233 for bulk sea-water. The atomic concentration ratios of C, O, Si, S, and Ca; Cl; and Mg and K for

234 the summertime sample were higher and lower than and similar to those of the wintertime sample,

235 respectively (also see Fig. S2, which clearly shows different distributions of individual particles

236 having specific elemental concentration ratios between the summertime and wintertime samples),

237 indicating that C, O, Si, S, and Ca; and Cl are enriched and depleted in the summertime sample,

respectively. In addition, those enriched and depleted elements have higher and lower concentration ratios than the bulk sea-water ratios, respectively.

As the [C]/[Na] ratios for both samples were high compared to bulk sea-water [C]/[Na] ratio, even the supermicron Antarctic SSAs contain significantly enriched organic species. The [C]/[Na] ratios of sample S1 were higher than those of sample S2, suggesting that the higher organic matter is related to the higher phytoplankton activities, and those for particles in the $PM_{1.0-2.5}$ fractions of samples S1 and S2 (1.12 and 0.83, respectively) were higher than $PM_{2.5-10}$ fractions (0.87 and 0.70, respectively), indicating that the smaller particles contain more organic species, which is consistent with other observations reporting more organics in the smaller SSAs (Quinn et al., 2015).

The [O]/[Na] ratios of sample S1 are higher than those of sample S2, and those for particles in the $PM_{2.5-10}$ fractions of samples S1 and S2 (0.77 and 0.68, respectively) are higher than the $PM_{1.0-2.5}$ fractions (0.71 and 0.66, respectively). Similar observations were made for S and Ca, for which the elemental concentration ratios were somewhat higher in sample S1 and in larger size fractions (see Table 1). In addition, the frequencies of encountering particles having higher [S]/[Na] or [Ca]/[Na] ratios than bulk sea-water were significantly higher in the summertime sample and in the larger size fractions (see encountering frequency data for S and Ca in Table 1), indicating that O, S, and Ca are interrelated with common sources, which is also supported by the observation of elongated $CaSO_4$ rods in the Raman and X-ray mapping measurements. The enriched S and O in the S1 sample appear to be due to the elevated $nss-SO_4^{2-}$ levels. In the austral summer (November–March) of the Antarctic, higher solar radiation levels and temperatures than the other seasons tend to enhance the phytoplankton activities (as supported by its high chlorophyll-*a* level for sample S1), which enhances the production and emission of oceanic dimethyl sulfide (DMS) (Wagenbach et al., 1998; Preunkert et al., 2008). The volatile DMS in the atmosphere undergoes complex sequences of gas-phase oxidation reactions, generating a range of sulfur-containing products, such as dimethyl sulfoxide (DMSO), methanesulfonic acid (MSA), SO_2, and H_2SO_4 (Gaston et al., 2010). These oxidized products can condense onto preexisting particles, resulting in the formation of $nss-SO_4^{2-}$-containing SSAs. As $CaSO_4$ can effloresce at very high RH, the $nss-SO_4^{2-}$ can combine easily with Ca, as observed in Figure 1, where the $CaSO_4$ rods are observed more frequently in sample S1.

9

268   Si is ==observed== for the summertime particles, and more abundantly ([Si]/[Na] = 0.03 vs.

269   0.01) and frequently (encountering frequency = 93.4 % vs. 47.5 %) in the $PM_{1.0-2.5}$ fraction than in

270   the $PM_{2.5-10}$ fraction. As Si is observed mostly in sample S1 and more in the smaller size fraction,

271   it appears to be from fragments of silica cell walls of diatoms, a major group of algae and a

272   common type of phytoplankton in the oceans (Litchman and Klausmeier, 2008; Alpert et al., 2015).

273   ==In the winter, the reduced diatom activities would decrease the emission of Si species into the==

274   ==atmosphere, resulting in the scarce observation of Si in the S2 sample.==

275   In the SSAs of samples S1 and S2, only Cl is depleted compared to bulk sea-water ([Cl]/[Na]

276   = 1.00 and 1.03 for samples S1 and S2, respectively, vs. 1.16 for sea-water), and the Cl depletion

277   is somewhat higher for the summertime SSAs than the wintertime and for $PM_{1.0-2.5}$ fractions than

278   $PM_{2.5-10}$ fractions, suggesting that Cl was liberated by the reactions of NaCl and/or $MgCl_2$ with

279   nss-SO_4^{2-} and/or $CH_3SO_3^-$, which are more abundant in the summer, with more depletion for

280   smaller SSAs having a higher surface to volume ratio and higher reactivity.

281

282   **3.2 Single-particle molecular speciation of Antarctic SSAs using RMS and ATR-FTIR**

283   **imaging**

284

285   Based on low-Z particle EPMA analysis, the C, O, Si, S, and Ca levels were elevated for

286   the summertime SSAs on a single-particle basis. This quantitative elemental X-ray analysis

287   provides useful information on their morphology, elemental chemical compositions, and mixing

288   states of individual Antarctica SSAs. On the other hand, as low-Z particle EPMA has a limitation

289   on molecular speciation and hydrogen detection, the RMS and ATR-FTIR imaging techniques

290   were applied in combination for the analysis of the same individual SSAs to investigate their

291   Raman- and IR-active organic and inorganic molecular species. Raman and ATR-FTIR techniques

292   are useful because their spectra of organic and inorganic compounds are quite specific depending

293   on their chemical species, phase, crystallinity, and neighboring environment. In particular, the

294   complicated vibrational spectral patterns observed in the fingerprint region (< 1500 cm^{-1}) in the

295   Raman and FTIR spectra can be critically useful for the positive or negative identification of

296   specific organic compounds with the same phase and crystallinity. In addition, the differences in

297   their spectra owing to their different signal generation mechanisms (i.e., scattering vs. absorption

298   of energy) and different selection rules would make the two fingerprint techniques rather

299   complementary (Jung et al., 2014).

300

301   **3.2.1 Organic species**

302   Among the ~250 individual SSAs of samples S1 and S2 investigated by RMS and ATR-

303   FTIR imaging techniques, the frequently observed organic species are most probably ones

304   containing Mg hydrate salts of alanine (MgAla) and Mg salts of fatty acids (MgFAs).

305   Figure 4 shows baseline-corrected Raman and ATR-FTIR spectra of two individual

306   summertime SSAs containing mainly two types of MgAla (detailed identification is given later.)

307   with some inorganic compounds. If several peaks from inorganic compounds (i.e., Raman peaks

308   at 124 and 467 cm^{-1} for SiO$_2$, at 717 and 1052 cm^{-1} for Mg(NO$_3$)$_2$, at 989 cm^{-1} for Na$_2$SO$_4$, at 1008

309   cm^{-1} for CaSO$_4$·2H$_2$O, and at 1068 cm^{-1} for NaNO$_3$; and ATR-FTIR peaks at 1087 and 1165 cm^{-1}

310   for SiO$_2$, at 1100 cm^{-1} for Na$_2$SO$_4$ and CaSO$_4$·2H$_2$O) are excluded from the consideration, the

311   Raman and ATR-FTIR spectra of two types of SSAs are similar except for their different Raman

312   and ATR-FTIR peak shapes. That is, the Raman peaks of crystalline water are sharp at 3276 and

313   3390 cm^{-1} for Type 1 SSA, compared to the relatively broad peak at 3410 cm^{-1} for Type 2 SSA.

314   The C-H vibration Raman peaks of Type 1 SSA are split at 3000/2988 cm^{-1} and 2940/2919 cm^{-1},

315   which correspond to the non-split Raman peaks of Type 2 SSA at 2989 cm^{-1} and 2939 cm^{-1}. The

316   C-H bending Raman peaks of Type 1 SSA are split into 1433/1457/1479 cm^{-1}, which correspond

317   to the Raman peaks of Type 2 SSA at 1427/1452 cm^{-1}. In the fingerprint region, the characteristic

318   Raman peaks both for Types 1 and 2 SSAs are observed at 869, 1102, 1130, 1254, ~1300, ~1370,

319   and 1640 cm^{-1}. Similarly, the ATR-FTIR peaks of crystal water are sharp and broad at 3265 and

320   3370 cm^{-1} for Type 1 SSA and 3372 cm^{-1} for Type 2 SSA, respectively, even though the C-H

321   vibration ATR-FTIR peaks are unclear for both types of SSAs. In the ATR-FTIR spectra, the water

322   bending peaks at ~1640 cm^{-1} are quite strong for both Types SSAs with the peak of Type 1 SSA

323   being much sharper. In the fingerprint region, the characteristic ATR-FTIR peaks for both Types 1

324   and 2 SSAs at 770, 869, 1127, 1254, 1312, ~1360, 1376, 1428, 1476, and 1507 cm^{-1} were sharp

325   and broad for the Type 1 and Type 2 SSAs, respectively. Similar Raman and ATR-FTIR peak

326   patterns of the Types 1 and 2 spectra except for their different peak shapes strongly indicates that

327   they have the same in chemical compositions but with different crystal structures. As amorphous

solids tend to provide broader Raman and ATR-FTIR peaks than crystalline solids (Shebanova and Lazor, 2003; Gouadec and Colomban, 2007; Lutz and Haeuseler, 1999; Yan et al., 2008), the Types 1 and 2 SSAs are most likely amorphous and crystalline solid particles, respectively.

Figure S3 shows the Raman and ATR-FTIR spectra of aerosols generated by the nebulization of a mixture solution of 0.2 M alanine and 0.1 M $MgCl_2$ standard chemicals and collected on Al foil. All the fresh aerosol particles immediately after nebulization showed the first pair of Raman and ATR-FTIR spectra in Figure S3 on a single particle basis, which resemble the Raman and ATR-FTIR spectra shown in Figure 4(b) when the Raman and ATR-FTIR peaks from the inorganic compounds are excluded. In particular, the ATR-FTIR spectra in Figure 4(b) and Figure S3 appear similar. When the aerosols were measured ~1 year later after the generated aerosols had been sealed in a plastic box and stored in a desiccator, approximately half of the generated aerosols showed a second pair of Raman and ATR-FTIR spectra, as shown in Figure S3, and the other half showed a third pair. The third spectra pair appears similar to those in Figure 4(a) for a crystalline solid SSA, whereas the second spectra pair appears to be between the first and third spectra pairs in Figure S3, strongly suggesting that the fresh aerosols generated from the alanine and $MgCl_2$ solution are a somewhat amorphous form of MgAla, whereas the second and third spectra pairs suggest a more crystalline nature of MgAla. The Raman peaks of the aerosols generated at 3409 and 1637 cm^{-1} are not from free water because these Raman peaks were unchanged even at very low RH (< 5%) when the in-situ Raman measurement was performed by changing the RH in the hygroscopic measurement system described in a previous study (Gupta et al., 2015). This means that the intensities and shapes of the Raman peaks should be reduced and changed, respectively, when the RH is decreased to a very low level if these peaks are from free water. In other words, the peaks are from the hydrate crystal water bound for divalent Mg compounds as the narrow peak shapes and peak positions resemble those of the known spectra of $MgCl_2 \cdot 6H_2O$ and $MgCl_2 \cdot 4H_2O$ solids with hydrate crystal water (Gupta et al., 2015). Divalent Ca ions are also present in sea-water. However, based on X-ray and Raman mapping results, Ca ions are mostly combined with inorganic SO_4^{2-} and slightly present in regions where organic moieties are.

Based on a comparison of the Raman and ATR-FTIR spectra obtained for the summertime SSAs and aerosols generated from the mixture solution of standard alanine and $MgCl_2$, the organic

species are ones containing mainly the Mg hydrate salts of alanine (MgAla), even though their precise molecular formula and the other possible minor components could not be confirmed. The Raman spectrum, which is the same as that of crystalline MgAla, was also observed for nascent SSAs produced using breaking waves, even though their molecular species were not identified (Ault et al., 2013b; Wang et al., 2015). In a previous study, the ATR-FTIR spectra were obtained from other summertime Antarctica SSAs, which appear very similar to that of amorphous MgAla (Maskey et al., 2011). Interestingly, almost all the ATR-FTIR spectra obtained in the previous work were for amorphous MgAla, whereas among the 254 individual SSAs analyzed in this study, the number of crystalline and amorphous MgAla-containing SSAs were 246 and 8, respectively, based on their Raman and ATR-FTIR spectra. How crystallization from SSAs occurred to form these organic Mg hydrate salts in the Antarctic environment is unclear because crystalline salts could not be made under very dry conditions and by oven-drying overnight. On the other hand, somewhat crystalline salts were encountered from the generated aerosol sample stored for ~ 1 year in a desiccator. Some efficient efflorescence seeds should be present in the Antarctic SSAs, which have much more complicated chemical compositions than the mixture solution of pure alanine and $MgCl_2$. The identification of an accurate molecular formula and structure of MgAla and an investigation of the crystallization mechanism requires further study.

The dominant dissolved amino acid in sea-water is glycine followed by alanine, aspartic acid or serine (Ogawa and Tanoue, 2003; Dittmar et al., 2001). In sea-water, MgAla species would be present as dissolved organic matter (DOM) in the form of alanine before being airborne. On the other hand, based on the Raman and ATR-FTIR spectra of standard powdery glycine and aerosol particles nebulized from aqueous mixtures of glycine/$MgCl_2$ and glycine/alanine/$MgCl_2$ as well as other common target chemicals for organic matter in nascent SSAs such as sodium dodecyl sulfate, a dipeptide of alanine and glycine, a polypeptide, and lipopolysaccharides, which are shown in Figure S4, it is clear that MgAla-containing SSAs are composed of mainly alanine with negligible glycine and other target chemicals. As the Raman and ATR-FTIR sensitivities for alanine and glycine are comparable and the same Raman spectrum for MgAla was also observed in the nascent SSAs produced from breaking waves, there must be some unknown processes for the generation of MgAla-containing SSAs from sea-water.

Figure 5 shows the baseline-corrected Raman and ATR-FTIR spectra of two individual

388   SSAs of sample S2 containing mainly MgFAs and both MgAla and MgFAs. As shown in Figure

389   S5, the Raman spectra of powdery standard Mg palmitate, palmitic acid, Mg stearate, and stearic

390   acid appear similar except for minor differences in relative peak intensities, which is not sufficient

391   to identify the organic species having the Raman spectrum of Figure 5(a). On the other hand, Mg

392   palmitate/stearate and palmitic/stearic acids have very different ATR-FTIR spectra as shown in

393   Figure S5. Owing to their additional strong peaks at ~1700 cm^{-1} for the -COOH functional group

394   and very different peak patterns in the fingerprint region of 700 – 1600 cm^{-1}, palmitic/stearic acids

395   can be clearly distinguishable from Mg palmitate/stearate. The ATR-FTIR spectrum of Mg

396   palmitate is different from that of Mg stearate based on the strong hydrate peaks at 3374 and 3256

397   cm^{-1} for Mg palmitate and the clearly different peak patterns in the wavenumber range, 1200 -

398   1600 cm^{-1}, between those of Mg palmitate and stearate. Figure S6 shows the ATR-FTIR spectra of

399   Mg palmitate, Mg stearate, a mixture of Mg palmitate and stearate (by 3:1), and MgFAs-containing

400   SSA, where the spectra of the mixture particle and the SSA match quite well, indicating that the

401   exemplar Antarctic SSA is a mixture of Mg palmitate and stearate. Therefore, this type of SSA is

402   called the Mg salts of fatty acids (MgFAs) above. The same Raman spectrum as that of MgFAs

403   was also observed for the nascent SSAs produced using breaking waves (Ault et al., 2013b; Wang

404   et al., 2015). As the pKa of palmitic and steric acids is 4.95, the palmitic/stearic acid moieties

405   degraded from the lipids would exist predominantly as surfactant palmitate/stearate in SSML

406   and/or on sea-surface and would crystallize as their Mg salts after the MgFAs-containing SSAs

407   were airborne by bubble busting.

408

409   **3.2.2 Inorganic species**

410

411   The Raman and IR active inorganic species observed in the Antarctic SSAs were $CaSO_4$,

412   Na_2SO_4, $NaNO_3$, $Mg(NO_3)_2$, NH_4NO_3, CH_3SO_3Mg (Mg methanesulfonate), and SiO_2 and their

413   standard Raman and ATR-FTIR spectra are shown in Figure S7. The inorganic species present in

414   the SSAs could be identified clearly by matching both the Raman and ATR-FTIR spectra of the

415   SSAs with those of the standard inorganic compounds, even though the inorganic species in the

416   SSAs were observed together with organic species so that the Raman and ATR-FTIR peaks of

417   inorganic species sometimes appear weak compared to those of organic species. On the other hand,

14

418   even under that situation, RMS is a powerful tool as the Raman peaks of inorganic compounds are
419   quite useful for identifying them.
420

421   **3.3 Single-particle characterization of Antarctic SSAs using RMS and ATR-FTIR imaging**
422

423   Table 2 shows relative encountering frequencies of the organic and inorganic species for
424   ~250 individual Antarctic SSAs. The encountering frequency of certain chemical species was
425   determined by counting the number of individual SSAs containing the species, regardless of its
426   content as the Raman and ATR-FTIR spectral data were used for qualitative molecular speciation.
427   Based on X-ray analysis, C and O were present in all the analyzed Antarctic SSAs. Indeed, organic
428   salt species were detected for all the particles of samples S1 and S2, showing that organic species
429   are ubiquitously present, even in supermicron SSAs. As shown in Table 2, organic salt species
430   were categorized into three groups containing (i) MgAla, (ii) MgFAs, and (iii) mixtures of the two
431   organic salts. The Raman and IR active inorganic salts were always observed together with organic
432   salt species, so that the relative encountering frequencies of inorganic species are shown in each
433   organic group.
434   All the particles of sample S1 contained only MgAla together with other inorganic species.
435   In particular, $CaSO_4$ and Na_2SO_4 are mixed almost internally with MgAla (for $PM_{1.0-2.5}$ and $PM_{2.5-10}$
436   fractions, the encountering frequencies of $CaSO_4$ were 98.3% and 92.9%, respectively, and those
437   of Na_2SO_4 were 98.3% and 88.6%, respectively), indicating that SO_4^{2-} is mostly in the form of a
438    $CaSO_4$ and Na_2SO_4 mixture. Although N X-ray signal was not detected probably due to the small
439   amount of NO_3^- present in the Antarctic SSAs, $Mg(NO_3)_2$ and $NaNO_3$ were frequently observed in
440   samples S1 and S2 using Raman and ATR-FTIR techniques. The nitrate in sea-water can be
441   generated by the photoammonification process, which transforms dissolved organic nitrogen
442   (DON) to labile inorganic nitrogen, mainly ammonium (NH_4^+) (Kitidis et al., 2006; Aarnos et al.,
443   2012; Xie et al., 2012; Rain-Franco et al., 2014; Paulot et al., 2015), followed by the microbial
444   oxidation of ammonium into nitrate (NO_3^-) by nitrifying bacteria (Carlucci et al., 1970; Hovanec
445   and Delong, 1996; Smith et al., 2014; Tolar et al., 2016). As the photoammonification depends on
446   solar radiations, the ammonium and nitrate production would be enhanced in the summer with
447   higher solar radiation level. Indeed, as shown in Table 2, nitrates are more frequently observed in

15

summertime sample S1 than wintertime sample S2. For the $PM_{1.0-2.5}$ and $PM_{2.5-10}$ fractions of sample S1, the overall encountering frequencies of $Mg(NO_3)_2$ are 51.7% and 77.1%, respectively, and those of $NaNO_3$ were 0.0% and 38.6%, respectively, where the NO_3^- moiety was observed more in the $PM_{2.5-10}$ fraction. The reason for why the NO_3^- moiety is more abundant in the $PM_{2.5-10}$ fraction is unclear. The SiO_2 concentration was 46.6% and 27.1% in the $PM_{1.0-2.5}$ and $PM_{2.5-10}$ fractions, respectively. SiO_2, which would be from fragments of silica cell walls of diatoms, appears to be in colloidal form because SiO_2 species are not water-soluble and were observed more in the $PM_{1.0-2.5}$ fraction than in $PM_{2.5-10}$. A small number of Mg methanesulfonate was observed only in the $PM_{1.0-2.5}$ fraction of sample S1. Higher phytoplankton activities in the summer enhance the production and emission of oceanic DMS, resulting in the production of MSA, which is a strong acid that can exist as an anion in sea-water and is observed as Mg salts in SSAs, even though its encountering frequency is not high compared to other sulfates.

A significant portion of SSAs of sample S2 contain only MgAla (overall 76.6% and 33.9% for $PM_{1.0-2.5}$ and $PM_{2.5-10}$ fractions, respectively) (see Table 2). Considering the encountering frequencies of MgAla mixed with MgFAs (21.9% and 54.8% for $PM_{1.0-2.5}$ and $PM_{2.5-10}$ fractions, respectively), MgAla is also almost ubiquitous in sample S2 (overall 98.5% and 88.7% for $PM_{1.0-2.5}$ and $PM_{2.5-10}$ fractions, respectively). MgFAs mixed internally with MgAla was encountered significantly in sample S2 (overall 23.5% and 66.1% for $PM_{1.0-2.5}$ and $PM_{2.5-10}$ fractions, respectively). For the $PM_{1.0-2.5}$ and $PM_{2.5-10}$ fractions, the encountering frequencies of $CaSO_4$ were 98.5% and 88.6% overall, respectively, whereas those of Na_2SO_4 were 26.6% and 8.0%, respectively, indicating that SO_4^{2-} is mostly in the form of $CaSO_4$. For the $PM_{1.0-2.5}$ and $PM_{2.5-10}$ fractions, the overall encountering frequencies of $Mg(NO_3)_2$ were 43.8% and 75.8%, respectively, and those of $NaNO_3$ were 12.5% and 27.4%, respectively, where the NO_3^- moiety was also observed more in the $PM_{2.5-10}$ fraction. SiO_2 was encountered much less frequently, 7.9% and 3.2% in the $PM_{1.0-2.5}$ and $PM_{2.5-10}$ fractions, respectively, compared to those of sample S1 (i.e., 46.6% and 27.1%, respectively). The observation of a higher encountering frequency of SiO_2 in sample S1 is consistent with that of X-ray analysis, where the detection of the Si X-ray signal was 70.1 % and. 0.7 % for samples S1 and S2, respectively.

The relative encountering frequency data for the organic and inorganic species of samples S1 and S2 clearly show their different chemical compositional features. MgAla-containing SSAs

16

are predominant for samples S1 and S2. The MgFAs were not observed in sample S1, but were observed in sample S2, mostly as internal mixtures with MgAla. As alanine is water-soluble and anions of fatty acids are surfactants, they would be present mostly at the bulk sea-water and SSML/sea-surface, respectively, before becoming airborne. Therefore, alanine- and fatty acids-containing SSAs are expected to be airborne through jet- and film-drop production during bubble busting, resulting in the generation of supermicron and submicron SSAs, respectively (de Leeuw et al., 2011; Quinn et al., 2015). In this study, supermicron SSAs were investigated for which MgAla is almost ubiquitous in samples S1 and S2, indicating that the supermicron SSAs were generated as jet-drops. As MgFAs was observed mostly together with MgAla in sample S2, the MgFAs-containing SSAs originating from film-drops might agglomerate with MgAla-containing supermicron SSAs in the air.

In a recent mesocosm experiment, the organic matter in SSAs generated from the wave braking of natural sea-water was monitored for 29 days after adding nutrients at the beginning of the experiment during which two phytoplankton blooms occurred (Wang et al., 2015). The aliphatic-rich organic matter level in the nascent SSAs was enhanced during the first bloom, whereas the oxygen-rich organic matter level increased at the early period of the experiment before the first bloom and remained somewhat constant thereafter, including the second bloom period. The MgAla and MgFAs observed in this study are the aliphatic-rich and oxygen-rich organic matters in their work, respectively, because the Raman spectra of MaAla and MgFAs are the same as those for oxygen- and aliphatic-rich organic matters and the O/C atomic ratios of alanine, palmitic, and stearic acids are 0.67, 0.13, and 0.11 (in their work, O/C > 0.5 for oxygen-rich organic matters and <0.25 for aliphatic-rich organic matters). In this study, the summertime Antarctic SSAs contain oxygen-rich organic matter, such as MgAla, whereas the wintertime SSAs contain aliphatic-rich organic matter, such as MgFAs as well as oxygen-rich organic matter. The aliphatic-rich organic matter was observed only during the first bloom in the mesocosm experiment, whereas supermicron MgFAs-containing SSAs were encountered only in the wintertime sample S2 collected during no bloom event, suggesting that the chemical features of organic matter in nascent SSAs cannot be correlated consistently with the phytoplankton activity. As microalgae can produce more lipid and less protein under environmental stress, such as limited nutrients and low temperature (Wu et al., 2011; Yu et al., 2009; Olson and Ingram, 1975), MgFAs, which were

508   biodegraded from lipid, may be observed more frequently in the wintertime oligotrophic Antarctic

509   Ocean with a lower temperature.

510

511   **4. Summary**

512   X-ray analysis of a single particle analysis showed that the supermicron summertime and

513   wintertime Antarctic samples have different elemental chemical compositions, even though all the

514   individual particles analyzed were SSAs; i.e., contents of C, O, Ca, S, and Si are more elevated,

515   whereas Cl is more depleted, for the summertime sample S1 than for the wintertime sample S2.

516   The combined application of RMS and ATR-FTIR imaging to the same individual SSAs made the

517   molecular speciation of the observed organic and inorganic species feasible. Based on qualitative

518   analysis of the chemical species present in the individual SSAs by RMS and ATR-FTIR imaging,

519   different organic species were observed in samples S1 and S2, i.e., Mg hydrate salts of alanine is

520   predominant in the S1 and S2 samples, whereas Mg salts of fatty acids mixed internally with Mg

521   hydrate salts of alanine are significant in sample S2. Although $CaSO_4$ are encountered significantly

522   in both samples S1 and S2, the other inorganic species, such as Na_2SO_4, $NaNO_3$, $Mg(NO_3)_2$, SiO_2,

523   and CH_3SO_3Mg were encountered more significantly in sample S1, suggesting that they reflect the

524   high phytoplankton activity in the summer.

525   In this study, there were new observations regarding the chemical compositional features

526   of nascent Antarctic SSAs and some of them need to be explained in further studies. First, although

527   just two SSA samples, having a high oceanic chlorophyll-*a* level contrast, collected in the summer

528   and winter were investigated, their chemical compositional features were clearly different in terms

529   of their chemical species and/or levels of inorganic and organic moieties. However, it is not clear

530   whether the different compositional features are due to the different sampling seasons or biological

531   activities. To answer this question, a study for overall 29 Antarctic aerosol samples collected

532   during Dec. 2011 and Sep. 2012 when the oceanic chlorophyll-*a* levels are in the range of 0.07-

533   13.38 µg/L is underway. Second, even the supermicron SSAs were enriched significantly by

534   organic matter, and thus the effects of organic matter in supermicron SSAs need to be considered

535   more seriously in a radiative forcing model study. Third, based on the Raman and ATR-FTIR

536   measurements, the organic moieties in SSAs are believed to be present mainly as the salt forms of

537   surprisingly simple organic compounds, such as alanine and palmitic/stearic acids, which appear

538 to be the biodegraded final products from proteins and lipids, respectively, but the reason for why

539 alanine and palmitic/stearic acids are predominant as the final products is unclear. In addition, the

540 Mg hydrate salts of alanine are almost ubiquitous in both the summertime and wintertime

541 supermicron SSAs but the Mg salts of fatty acids were encountered only in the wintertime

542 supermicron SSAs, which will require further study to better understand the generation processes

543 of Antarctic SSAs.

544

545 **Acknowledgements**

549

550 **References**

551

552 Aarnos, H., Ylöstalo, P., and Vähätalo, A. V.: Seasonal phototransformation of dissolved organic

553   matter to ammonium, dissolved inorganic carbon, and labile substrates supporting

554   bacterial biomass across the Baltic Sea, J. Geophys. Res., 2012, 117, G01004, doi:10.

555   1029/2010JG001633.

556 Alpert, P. A., Kilthau, W. P., Bothe, D. W., Radway, J. C., Aller, J. Y., and Knopf, D. A.: The

557   influence of marine microbial activities on aerosol production: A laboratory mesocosm

558   study, J. Geophys. Res., 2015, 10.1002/2015JD023469.

559 Ault, A. P., Moffet, R. C., Baltrusaitis, J., Collins, D. B., Ruppel, M. J., Cuadra-Rodriguez, L. A.,

560   Zhao, D., Guasco, T. L., Ebben, C. J., Geiger, F. M., Bertram, T. H., Prather, K. A., and

561   Grassian, V. H.: Size-Dependent Changes in Sea Spray Aerosol Composition and

562   Properties with Different Seawater Conditions, Environ. Sci. Technol., 2013a, 47, 5603−

563   5612.

564 Ault, A. P., Zhao, D., Ebben, C. J., Tauber, M. J., Geiger, F. M., Prather, K. A., and Grassian, V.

565   H.: Raman microspectroscopy and vibrational sum frequency generation spectroscopy as

566   probes of the bulk and surface compositions of size-resolved sea spray aerosol particles,

567   Phys.Chem. Chem. Phys., 2013b, 15, 6206-6212.

568   Bates, T. S., Quinn, P. K., Frossard, A. A., Russell, L. M., Hakala, J., Petäjä, T., Kulmala, M.,

569   Covert, D. S., Cappa, C. D., Li, S. M., Hayden, K. L., Nuaaman, I., McLaren, R., Massoli,

570   P., Canagaratna, M. R., Onasch, T. B., Sueper, D., Worsnop, D. R., and Keene, W. C.:

571   Measurements of ocean derived aerosol off the coast of California, J. Geophys. Res.:

572   Atmos. 2012, 117, D00V15.

573   Biancato, D., Ceccato, D., Chiminello, F., and Mittner, P.: Micro-PIXE and principal component

574   analysis in a study of internal mixing phenomena in Antarctic coastal aerosol, Nucl. Instr.

575   Meth. Phys. Res. B, 2006, 249, 561-565.

576   Carlucci, A. F., Hartwig, E. O., and Bowes, P. M.: Biological production of nitrite in seawater, Mar.

577   Biol., 1970, 7, 161-166.

578   de Leeuw, G., Andreas, E' L', Anguelova, M. D., Fairall, C. W., Lewis, E. R., O′Dowd, C., Schulz,

579   M., and Schwartz, S. E.: Production flux of sea spray aerosol, Rev. Geophys., 2011, 49,

580   RG2001, doi:10.1029/2010RG000349.

581   Dittmar, T., Fitznar, H. P., and Kattner, G.: Origin and biogeochemical cycling of organic nitrogen

582   in the eastern Arctic Ocean as evident from D- and L-amino acids. Geochim. Cosmochim.

583   Acta, 2001, 65, 4103–4114.

584   Eom, H.-J., Jung, H.-J., Sobanska, S., Chung, S.-G., Son, Y.-S., Kim, J.-C., Sunwoo, Y., and Ro,

585   C.-U.: Iron speciation of airborne subway particles by the combined use of energy

586   dispersive electron probe X-ray microanalysis and Raman microspectrometry, Anal.

587   Chem., 2013, 85, 10424-10431.

588   Gaston, C. J., Pratt, K. A., Qin, X., and Prather, K. A.: Real-time detection and mixing state of

589   methanesulfonate in single particles at an inland urban location during a phytoplankton

590   bloom, Environ. Sci. Technol., 2010, 44, 1566–1572.

591   Gouadec, G. and Colomban, P.: Raman Spectroscopy of Nanomaterials: How Spectra Relate to

592   Disorder, Particle Size and Mechanical Properties, Prog. Cryst. Growth Charact. Mater.,

593   2007, 53, 1−56.

594   Gupta, D., Eom, H.-J., Cho, H.-R., and Ro, C.-U.: Hygroscopic behavior of NaCl–MgCl$_2$ mixture

595   particles as nascent sea-spray aerosol surrogates and observation of efflorescence during

596   humidification, Atmos. Chem. Phys., 2015, 15, 11273-11290.

597   Hara, K., Osada, K., Kido, M., Matsunaga, K., Iwasaka, Y., Hashida, G., and Yamanouchi, T.:

598   Variations of constituents of individual sea-salt particles at Syowa station, Antarctica,

599   Tellus, 2005, 57B, 230-246.

600 Hara, K., Iwasaka, Y., Wada, M., Ihara, T., Shiba, H., Osada, K., and Yamanouchi, T.: Aerosol

601   constituents and their spatial distribution in the free troposphere of coastal Antarctic

602   regions, J. Geophys. Res., 2006, 111, D15216.

603 Hara, K., Osada, K., Yabuki, M., and Yamanouchi, T.: Seasonal variation of fractionated sea-salt

604   particles on the Antarctic coast, Geophys. Res. Lett., 2012, 39, L18801.

605 Hara, K., Osada, K., and Yamanouchi, T.: Tethered balloon-borne aerosol measurements: seasonal

606   and vertical variations of aerosol constituents over Syowa Station, Antarctica, Atmos.

607   Chem. Phys., 2013, 13, 9199-9139.

608 Hara, K., Nakazawa, F., Fujita, S., Fukui, K., Enomoto, H., and Sugiyama, S.: Horizontal

609   distributions of aerosol constituents and their mixing states in Antarctica during the JASE

610   traverse, Atmos. Chem. Phys., 2014, 14, 10211-10230.

611 Haynes, W. M.: CRC Handbook of Chemistry and Physics, 96th Edition, CRC Press, 2015, pp.

612   14-18.

613 Hovanec, T. A. and DeLong, E. F.: Comparative Analysis of Nitrifying Bacteria Associated with

614   Freshwater and Marine Aquaria, Appl. Environ. Microb., 1996, 62(8), 2888-2896.

615 Hu, Q.-H., Xie, Z.-Q., Wang, X.-M., Kang, H., He, Q.-F., and Zhang, P.: Secondary organic

616   aerosols over oceans via oxidation of isoprene and monoterpenes from Arctic to Antarctic,

617   Sci. Rep., 2013, 3, 2280.

618 Jung, H.-J., Eom, H.-J., Kang, H.-W., Moreau, M., Sobanska, S., and Ro, C.-U.: Combined use of

619   quantitative ED-EPMA, Raman microspecrometry, and ATR-FTIR imaging techniques

620   for the analysis of individual particles, Analyst, 2014, 139, 3949-3960.

621 Kerminen, V.-M., Teinilä, K., and Hillamo, R.: Chemistry of sea-salt particles in the summer

622   Antarctic atmosphere, Atmos. Environ., 2000, 34, 2817–2825.

623 Kitidis, V., Uher, G., Upstill-Goddard, R. C., Mantoura, R. F. C., Spyres, G., and Woodward, E.

624   M. S.: Photochemical production of ammonium in the oligotrophic Cyprus Gyre (Eastern

625   Mediterranean), Biogeosciences, 2006, 3, 439–449.

626 Laskina, O.: Physicochemical properties of mineral dust and sea spray aerosols, Ph. D. thesis, 2015,

627   129-149.

628 Lee, S. H., Joo, H. M., Joo, H., Kim, B. K., Song, H. J., Jeon, M., and Kang, S.-H.: Large
629   contribution of small phytoplankton at Marian Cove, King George Island, Antarctica,
630   based on long-term monitoring from 1996 to 2008, Polar Biol., 2015, 38, 207-220.

631 Litchman, E. and Klausmeier, C. A.: Trait-Based Community Ecology of Phytoplankton, Annu.
632   Rev. Ecol. Evol. Syst., 2008, 39, 615-639.

633 Lutz, H. D. and Haeuseler, H.: Infrared and Raman spectroscopy in inorganic solids research, J.
634   Mol. Struct., 1999, 511−512, 69−75.

635 Maskey, S., Geng, H., Song, Y.-C., Hwang, H., Yoon, Y.-J., Ahn, K.-H., and Ro, C.-U.: Single-
636   Particle Characterization of Summertime Antarctic Aerosols Collected at King George
637   Island Using Quantitative Energy-Dispersive Electron Probe X-ray Microanalysis and
638   Attenuated Total Reflection Fourier Transform-Infrared Imaging Techniques, Environ. Sci.
639   Technol., 2011, 45, 6275–6282.

640 O'Dowd, C. D., Facchini, M. C., Cavalli, F., Ceburnis, D., Mircea, M., Decesari, S., Fuzzi, S.,
641   Yoon, Y. J., and Putaud, J.-P.: Biogenically driven organic contribution to marine aerosol,
642   Nature, 2004, 431, 676-680.

643 Olson, G. J. and Ingram, L. O.: Effects of temperature and nutritional changes on the fatty acids
644   of Agmenellum quadruplicatum, J. Bacteriol., 1975, 124, 373-379.

645 Ogawa, H. and Tanoue, E.: Dissolved Organic Matter in Oceanic Waters, J. Oceanogr., 2003, 59,
646   129-147.

647 Paulot, F., Jacob, D. J., Johnson, M. T., Bell, T. G., Baker, A. R., Keene, W. C., Lima, I. D., Doney,
648   S. C., and Stock, C. A.: Global oceanic emission of ammonia: Constraints from seawater
649   and atmospheric observations, Global Biogeochem. Cycles, 29, 1165–1178.

650 Prather, K. A., Bertram, T. H., Grassian, V. H., Deane, G. B., Stokes, M. D., DeMott, P. J.,
651   Aluwihare, L. I., Palenik, B. P., Azam, F., Seinfeld, J. H., Moffet, R. C., Molina, M. J.,
652   Cappa, C. D., Geiger, F. M., Roberts, G. C., Russell, L. M., Ault, A. P., Baltrusaitis, J.,
653   Collins, D. B., Corrigan, C. E., Cuadra-Rodriguez, L. A., Ebben, C. J., Forestieri, S. D.,
654   Guasco, T. L., Hersey, S. P., Kim, M. J., Lambert, W. F., Modini, R. L., Mui, W., Pedler,
655   B. E., Ruppel, M. J., Ryder, O. S., Schoepp, N. G., Sullivan, R. C., and Zhao, D.: Bringing
656   the ocean into the laboratory to probe the chemical complexity of sea spray aerosol, Proc.
657   Natl. Acad. Sci. USA., 2013, v110, 19, 7550–7555.

658 Préndez, M., Wachter, J., Vega, C., Flocchini, R. G., Wakayabashi, P., and Morales, J. R.: PM$_{2.5}$

659   aerosols collected in the Antarctic Peninsula with a solar powered sampler during austral

660   summer periods, Atmos. Environ., 2009, 43, 5575–5578.

661 Preunkert, S., Jourdain, B., Legrand, M., Udisti, R., Becagli, S., and Cerri, O.: Seasonality of sulfur

662   species (dimethyl sulfide, sulfate, and methanesulfonate) in Antarctica: Inland versus

663   coastal regions, J. Geophys. Res., 2008, 113, D15302

664 Quinn, P. K., Bates, T. S., Schulz, K. S., Coffman, D. J., Frossard, A. A., Russell, L. M., Keene, W.

665   C., and Kieber, D. J.: Contribution of sea surface carbon pool to organic matter enrichment

666   in sea spray aerosol, Nat. Geosci., 2014, 7, 228–232.

667 Quinn, P. K., Collins, D. B., Grassian, V. H., and Prather, K. A.: Chemistry and Related Properties

668   of Freshly Emitted Sea Spray Aerosol, Chem. Rev., 2015, 115, 4383−4399.

669 Rain-Franco, A., Muñoz, C., Fernandez, C.: Ammonium Production off Central Chile (36°S) by

670   Photodegradation of Phytoplankton-Derived and Marine Dissolved Organic Matter, Plos

671   One, 2014, 26, 9(6), e100224, doi:10.1371/journal.pone.0100224.

672 Rinaldi, M., Decesari, S., Finessi, E., Giulianelli, L., Carbone, C., Fuzzi, S., O'Dowd, C. D.,

673   Ceburnis, D., and Facchini, M. C.: Primary and Secondary Organic Marine Aerosol and

674   Oceanic Biological Activity: Recent Results and New Perspectives for Future Studies, Adv.

675   Meteorol., 2010, 310682, 1-10.

676 Ro, C.-U., Osán, J., Szalóki, I., de Hoog, J., Worobiec, A., and Van Grieken, R.: A Monte Carlo

677   program for quantitative electron-induced X-ray analysis of individual particles, Anal.

678   Chem., 2003, 75, 851–859.

679 Ro, C.-U., Hwang, H., Kim, H., Chun, Y., and Van Grieken, R.: Single-particle characterization of

680   four "Asian dust" samples collected in Korea, using low-Z particle electron probe X-ray

681   microanalysis, Environ. Sci. Technol., 2005, 39, 1409–1419.

682 Ro, C.-U., Osán, J., and Van Grieken, R.: Determination of low-Z elements in individual

683   environmental particles using windowless EPMA, Anal. Chem., 1999, 71, 1521–1528.

684 Schindelholz, E., Risteen, B. E., and Kelly, R. G.: Effect of Relative Humidity on Corrosion of

685   Steel under Sea Salt Aerosol Proxies, J. Electrochem. Soc., 2014, 161 (10), C460-470.

686 Schloss, I. R., Wasilowska, A., Dumont, D., Almandoz, G. O., Hernando, M. P., Michaud-Tremblay,

687   C.-A., Saravia, L., Rzepecki, M., Monien, P., Monien, D., Kopczyńska, E. E., Bers, A. V.,

688   Ferreyra, G. A.: On the phytoplankton bloom in coastal waters of southern King George
689   Island (Antarctica) in January 2010: An exceptional feature?, Limnol. Oceanogr., 2014,
690   59(1), 195-210.

691 Shebanova, O. N. and Lazor, P. J.: Raman spectroscopic study of magnetite ($FeFe_2O_4$): a new
692   assignment for the vibrational spectrum, Solid State Chem., 2003, 174, 424−430.

693 Smith, J. M., Chavez, F. P., and Francis, C. A.: Ammonium Uptake by Phytoplankton Regulates
694   Nitrification in the Sunlit Ocean, Plos One, 24, 9(9), e108173. doi:10.1371/journal.pone.
695   0108173.

696 Sobanska, S., Hwang, H., Choël, M., Jung, H.-J., Eom, H.-J., Kim, H., Barbillat, J., and Ro, C.-U.:
697   Investigation of the Chemical Mixing State of Individual Asian Dust Particles by the
698   Combined Use of Electron Probe X-ray Microanalysis and Raman Microspectrometry,
699   Anal. Chem., 2012, 84, 3145−3154.

700 Song, Y.-C., Ryu, J., Malek, M. A., Jung, H.-J., and Ro, C.-U.: Chemical speciation of individual
701   airborne particles by the combined use of quantitative energy-dispersive electron probe
702   X-ray microanalysis and attenuated total reflection Fourier transform-infrared imaging
703   techniques, Anal. Chem., 2010, 82, 7987–7998.

704 Song, Y.-C., Eom, H.-J., Jung, H.-J., Malek, M. A., Kim, H. K., Geng, H., and Ro, C.-U.:
705   Investigation of aged Asian dust particles by the combined use of quantitative ED-
706   EPMA and ATR-FTIR imaging, Atmos. Chem. Phys., 2013, 13, 3463-3480.

707 Tolar, B. B., Ross, M. J., Wallsgrove, N. J., Liu, Q., Aluwihare, L. I., Popp, B. N., and Hollibaugh,
708   J. T.: Contribution of ammonia oxidation to chemoautotrophy in Antarctic coastal waters,
709   ISME. J., 2016, 1-15.

710 Van Dalen, G., Heussen, P. C. M., Den Adel, R., and Hoeve, R. B. J.: Attenuated total internal
711   reflection infrared microscopy of multilayer plastic packaging foils, Appl. Spectrosc.,
712   2007, 61, 593–602.

713 Vekemans, B., Janssens, K., Vincze, L., Adams, F., and Van Espen, P.: Analysis of X-ray spectra
714   by iterative least squares (AXIL): New developments, X-Ray Spectrom., 1994, 23, 278–
715   285.

716 Wagenbach, D., Ducroz, F., Mulvaney, R., Keck, L., Minikin, A., Legrand, M., Hall, J. S., and
717   Wolff, E. W.: Sea-salt aerosol in coastal Antarctic regions, J. Geophys. Res., 1998, 103,

718   10961−10974.

719 Wang, X., Sultana, C. M., Trueblood, J., Hill, T. C. J., Malfatti, F., Lee, C., Laskina, O., Moore,

720   K. A., Beall, C. M., McCluskey, C. S., Cornwell, G. C., Zhou, Y., Cox, J. L., Pendergraft,

721   M. A., Santander, M. V., Bertram, T. H., Cappa, C. D., Azam, F., DeMott, P. J., Grassian,

722   V. H., and Prather, K. A.: Microbial Control of Sea Spray Aerosol Composition: A Tale

723   of Two Blooms, ACS Cent. Sci., 2015, 1, 124−131.

724 Wu, H., Volponi, J. V., Oliver, A. E., Parikh, A. N., Simmons, B. A., and Singh, S.: In vivo

725   lipidomics using single-cell Raman spectroscopy, Proc. Natl. Acad. Sci. USA., 2011, 108,

726   3809-3814.

727 Xiao, H.-S., Dong, J.-L., Wang, L.-Y., Zhao, L.-J., Wang, F., and Zhang, Y.-H.: Spatially resolved

728   micro-Raman observation on the phase separation of effloresced sea salt droplets, Environ.

729   Sci. Technol., 2008, 42, 8698-8702.

730 Xie, H., Bélanger, S., Song, G., Benner, R., Taalba, A., Blais, M., Tremblay, J.-É., and Babin, M.:

731   Photoproduction of ammonium in the southeastern Beaufort Sea and its biogeochemical

732   implications, Biogeosciences, 2012, 9, 3047–3061.

733 Yan, J., Asami, T., and Kuriyagawa, T.: Nondestructive measurement of machining-induced

734   amorphous layers in single-crystal silicon by laser micro-Raman spectroscopy, Precision

735   Eng., 2008, 32, 186−195.

736 Yu, E. T., Zendejas, F. J., Lane, P. D., Gaucher, S., Simmons, B. A., and Lane, T. W.: Triacylglycerol

737   accumulation and profiling in the model diatoms Thalassiosira pseudonana and

738   Phaeodactylum tricornutum (Baccilariophyceae) during starvation, J. Appl. Phycol., 2009,

739   21, 669-681.

Table 1. Atomic concentration ratios of the chemical elements to Na for individual particles in the summertime and wintertime $PM_{2.5-10}$ and $PM_{1.0-2.5}$ fractions.

sample		Summertime sample S1		Wintertime sample S2	
size fraction		$PM_{1.0-2.5}$ (stage 3)	$PM_{2.5-10}$ (stage 2)	$PM_{1.0-2.5}$ (stage 3)	$PM_{2.5-10}$ (stage 2)
number of particles analyzed		146	148	154	156
average size (μm)		2.0 (±0.6)	2.9 (±1.5)	1.7 (±0.8)	3.2 (±1.5)
Elemental ratios	Sea-water ratios in atomic conc.*	Atomic concentration ratios			
[C]/[Na]	0.01	1.12 (±0.35)	0.87 (±0.33)	0.83 (±0.33)	0.70 (±0.24)
[O]/[Na]	114.03**	0.71 (±0.23)	0.77 (±0.25)	0.66 (±0.22)	0.68 (±0.24)
[Mg]/[Na]	0.11	0.09 (±0.02)	0.11 (±0.04)	0.11 (±0.03)	0.10 (±0.03)
[Cl]/[Na]	1.16	0.98 (±0.05)	1.01 (±0.05)	1.02 (±0.10)	1.04 (±0.04)
[K]/[Na]	0.02	0.02 (±0.01)	0.02 (±0.01)	0.01 (±0.01)	0.02 (±0.01)
[S]/[Na]	0.06	0.065 (±0.015)	0.070 (±0.019)	0.058 (±0.013)	0.059 (±0.016)
[Ca]/[Na]	0.02	0.022 (±0.009)	0.027 (±0.011)	0.018 (±0.029)	0.023 (±0.012)
[Si]/[Na]	0.00	0.03 (±0.02)	0.01 (±0.01)	0.00	0.00
Encountering frequency of particles with [S]/[Na] > 0.06		52.7%	69.7%	43.8%	41.9%
Encountering frequency of particles with [Ca]/[Na] > 0.02		48.4%	69.7%	31.5%	48.6%
Encountering frequency of particles with [Si]/[Na] > 0.00		93.4%	47.5%	-	-
* refs. : Haynes, W. M., 2015; Hara et al., 2005 ** [O]/[Na] value for sea-water is not meaningful as H_2O content in sea-water is considered.					

Table 2. Relative encountering frequencies (in %) of the organic and inorganic species of individual summertime and wintertime SSAs.

Organic salt group	sample	Summertime sample S1		Wintertime sample S2	
	size fraction	$PM_{1.0-2.5}$ (stage 3)	$PM_{2.5-10}$ (stage 2)	$PM_{1.0-2.5}$ (stage 3)	$PM_{2.5-10}$ (stage 2)
	number of particles analyzed	58	70	64	62
containing Mg hydrate salts of alanine (MgAla)	overall	100.0	100.0	76.6	33.9
	with $CaSO_4$	98.3	92.9	76.6	29.0
	with Na_2SO_4	98.3	88.6	18.8	4.8
	with $Mg(NO_3)_2$	51.7	77.1	32.8	22.6
	with NH_4NO_3	3.4	-	6.3	-
	with $NaNO_3$	-	38.6	7.8	14.5
	with Mg methanesulfonate	3.4			
	with SiO_2	46.6	27.1	6.3	1.6
containing Mg salts of fatty acids (MgFAs)	overall			1.6	11.3
	with $CaSO_4$			1.6	6.4
	with $Mg(NO_3)_2$			1.6	3.2
containing both MgAla and MgFAs	overall			21.9	54.8
	with $CaSO_4$			20.3	53.2
	with Na_2SO_4			7.8	3.2
	with $Mg(NO_3)_2$			9.4	50.0
	with NH_4NO_3			1.6	-
	with $NaNO_3$			4.7	12.9
	with SiO_2			1.6	1.6

Figure 1. Typical secondary electron images (SEIs) of aerosol particles on stages 2 of the austral (a) summertime and (b) wintertime samples collected at King Sejong station, Antarctica.

Figure 2. Secondary electron, molecular Raman map, and elemental X-ray map (overlaid on SEIs) images of two typical (a) summertime and (b) wintertime SSAs.
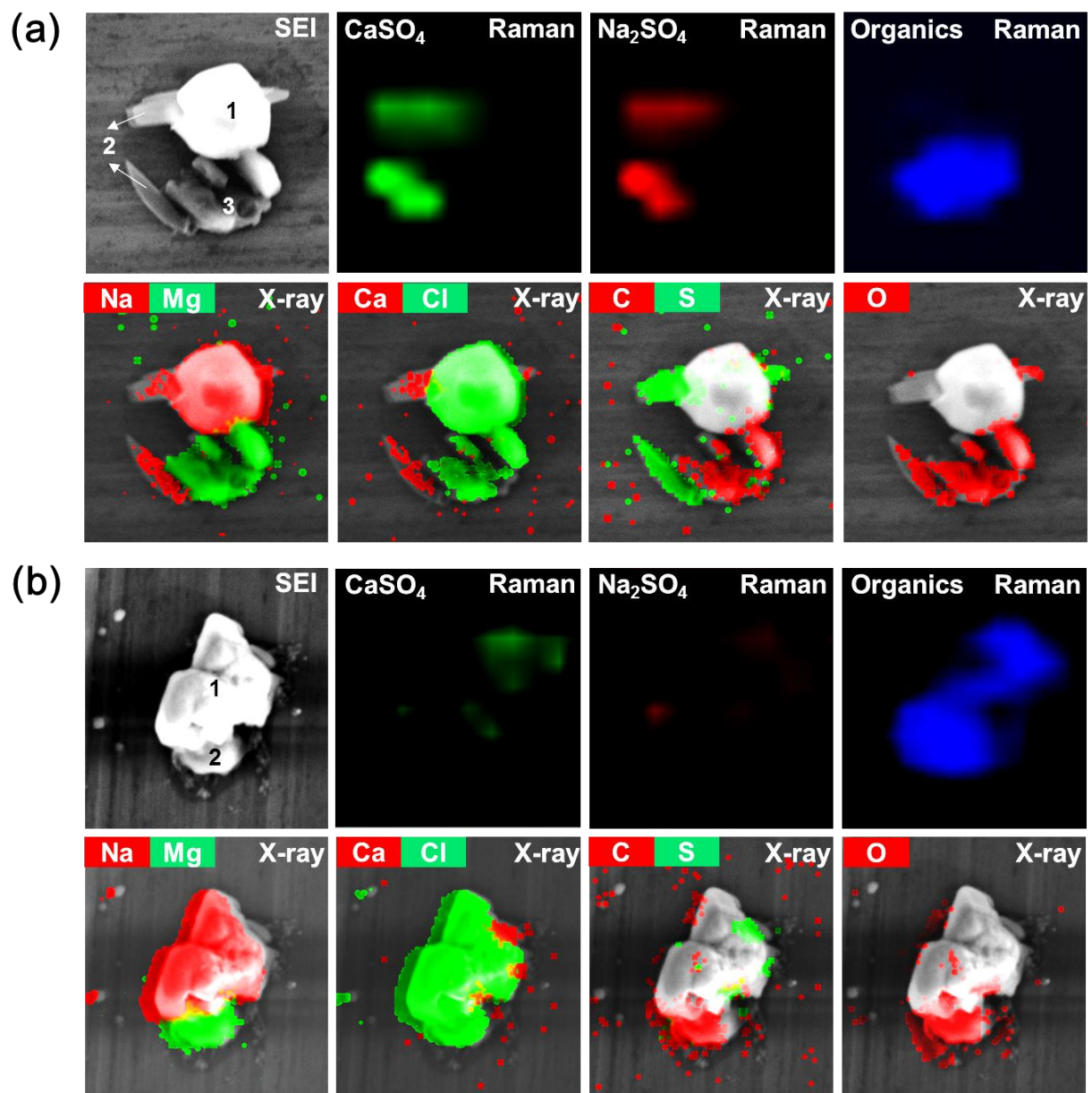
Figure 3. X-ray spectra and elemental atomic concentrations (in atomic %) of (a) the summertime and (b) wintertime SSA particles shown in Figure 2.
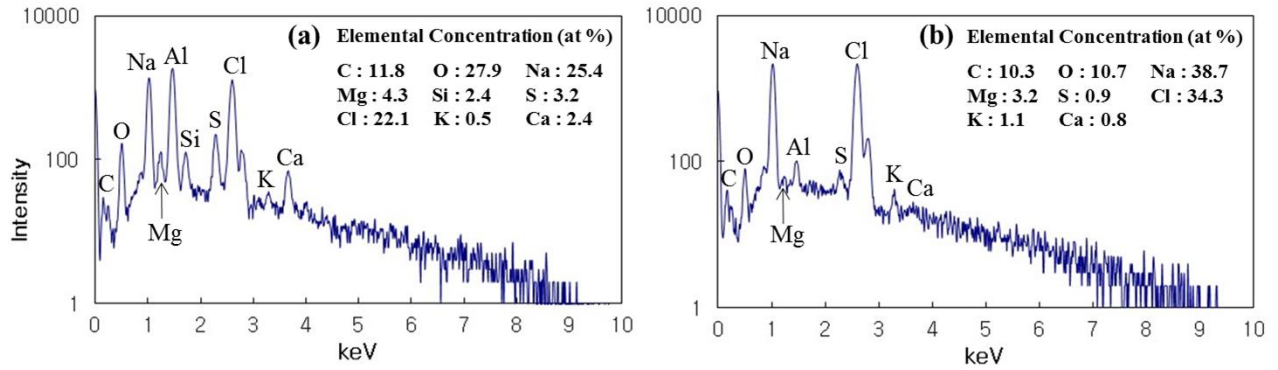
Figure 4. Raman and ATR-FTIR spectra of two typical individual summertime SSAs. The ATR-FTIR data from the 2200–2390 cm^{-1} region, where the atmospheric CO_2 peaks are present, were deleted for clarity.
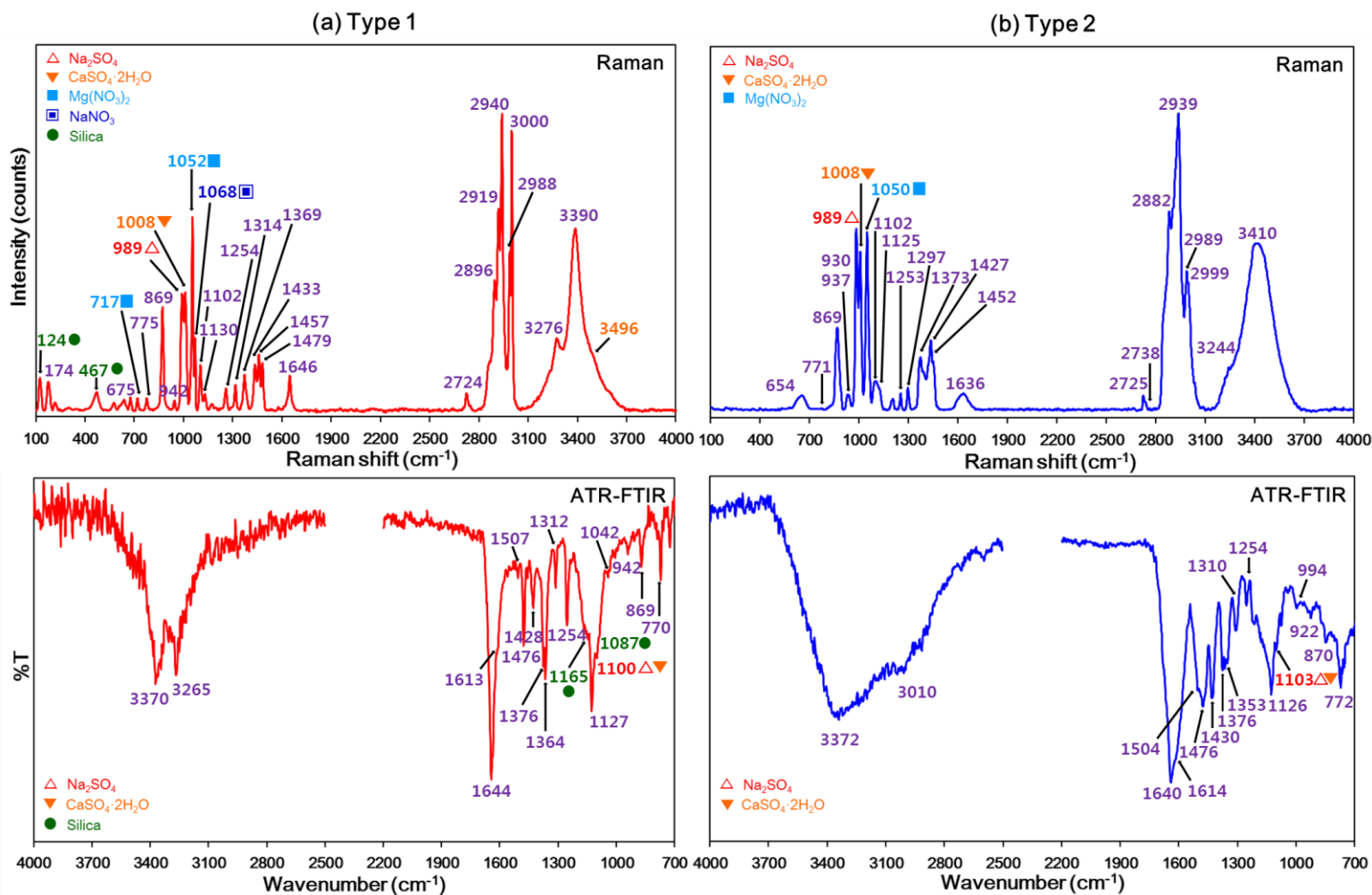
Figure 5. Raman and ATR-FTIR spectra of two typical individual wintertime SSAs. The ATR-FTIR data from the 2200–2390 cm^{-1} region, where atmospheric CO_2 peaks are present, were deleted for clarity.
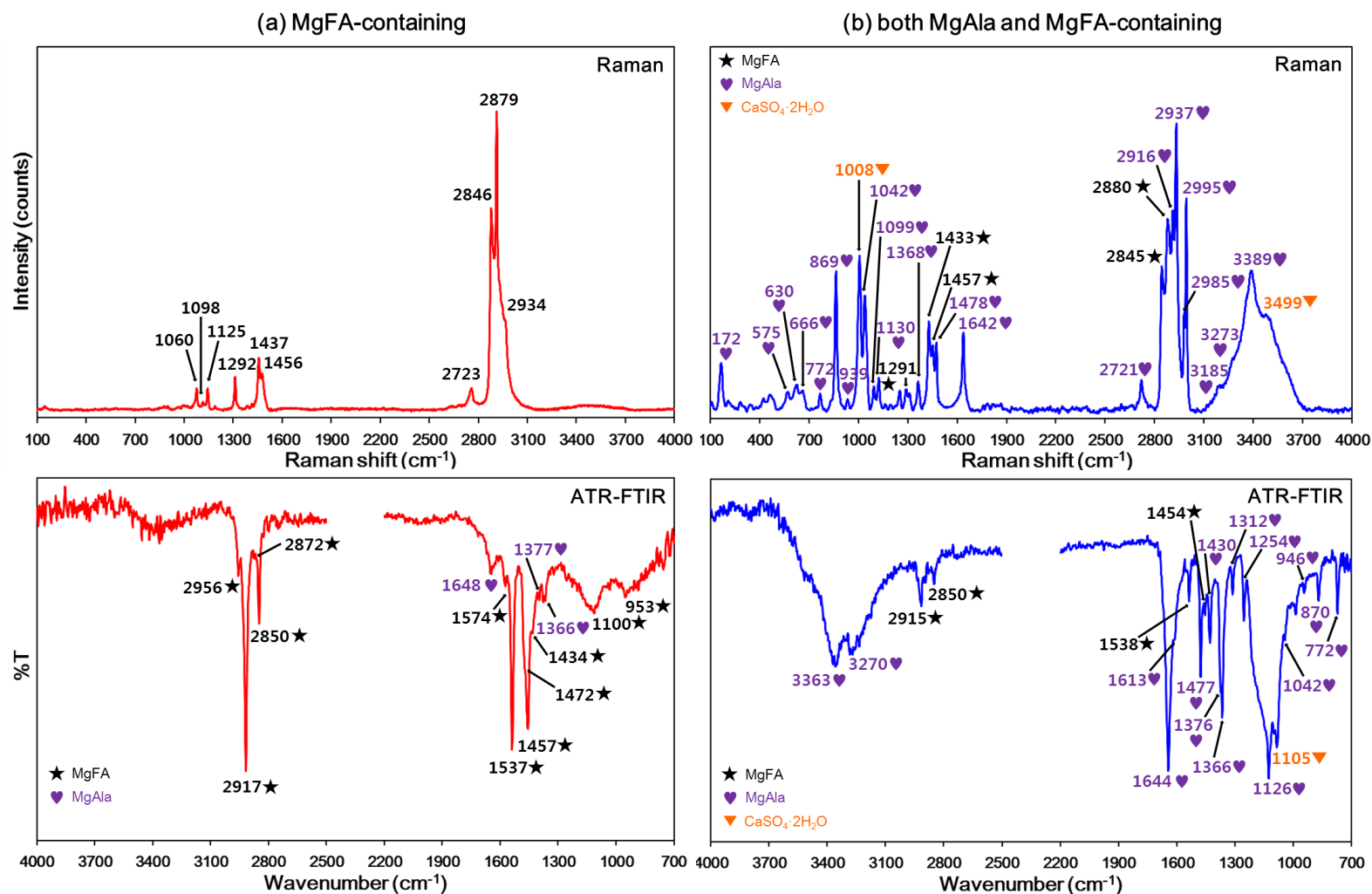
Supplementary Information for publication

Single-particle investigation of summertime and wintertime Antarctic sea spray aerosols using low-*Z* particle EPMA, Raman microspectrometry, and ATR-FTIR imaging techniques

Hyo-Jin Eom[1], Dhrubajyoti Gupta[1], Hye-Rin Cho[1], HeeJin Hwang[2], SoonDo Hur[2], Yeontae Gim[3] and Chul-Un Ro[1,†]

[1]*Department of Chemistry, Inha University, Incheon, Republic of Korea*
[2]*Polar Climate Change Research Division, Korea Polar Research Institute, Incheon, Republic of Korea*
[3]*Arctic Research Center, Korea Polar Research Institute, Incheon, Republic of Korea*

[†]*Corresponding author. Tel.: +82 32 860 7676; fax: +82 32 874 9207*
E-mail address: curo@inha.ac.kr (C.-U. Ro)

Table S1. Average elemental concentrations of individual particles in summertime and wintertime $PM_{2.5-10}$ and $PM_{1.0-2.5}$ fractions using low-Z particle EPMA.

sample	Summertime sample S1				Wintertime sample S2			
size fraction	$PM_{1.0-2.5}$ (stage 3)		$PM_{2.5-10}$ (stage 2)		$PM_{1.0-2.5}$ (stage 3)		$PM_{2.5-10}$ (stage 2)	
number of particles	146		148		154		156	
average size (μm)	2.0 ($\pm$0.6)		2.9 ($\pm$1.5)		1.7 ($\pm$0.8)		3.2 ($\pm$1.5)	
element	at. conc. (%)	wt. conc. (%)	at. conc. (%)	wt. conc. (%)	at. conc. (%)	wt. conc. (%)	at. conc. (%)	wt. conc. (%)
C	27.1 ($\pm$4.8)	14.6	21.9 ($\pm$5.9)	11.5	21.6 ($\pm$5.1)	11.2	18.8 ($\pm$3.8)	9.6
O	17.3 ($\pm$3.2)	12.4	19.5 ($\pm$4.7)	13.6	17.4 ($\pm$3.2)	12.0	18.2 ($\pm$4.0)	12.3
Na	25.2 ($\pm$3.3)	25.9	26.1 ($\pm$3.4)	26.2	27.6 ($\pm$4.2)	27.3	28.3 ($\pm$4.0)	27.5
Mg	2.3 ($\pm$0.4)	2.5	2.7 ($\pm$0.7)	2.9	2.9 ($\pm$0.5)	3.0	2.7 ($\pm$0.6)	2.8
Si	0.8 ($\pm$0.5)	1.0	0.3 ($\pm$0.4)	0.4	0.0	0.0	0.0	0.0
S	1.6 ($\pm$0.3)	2.3	1.8 ($\pm$0.5)	2.5	1.6 ($\pm$0.2)	2.2	1.6 ($\pm$0.3)	2.2
Cl	24.8 ($\pm$3.7)	39.4	26.4 ($\pm$3.4)	40.9	28.1 ($\pm$4.1)	42.8	29.2 ($\pm$3.8)	43.8
K	0.5 ($\pm$0.2)	0.9	0.5 ($\pm$0.2)	0.9	0.4 ($\pm$0.3)	0.7	0.5 ($\pm$0.2)	0.8
Ca	0.6 ($\pm$0.2)	1.1	0.7 ($\pm$0.3)	1.2	0.5 ($\pm$0.6)	0.9	0.6 ($\pm$0.3)	1.0

Figure S1. Three-day (72 h) backward air mass trajectories at 500 m-, 1000 m- and 1500 m-receptor heights in December 9, 2011 and July 23, 2012. HYbrid Lagrangian Single-Particle Integrated Trajectory (HYSPLIT) model available at the NOAA Air Resources Laboratory's web server (http: //www.arl.noaa.gov/ready/hysplit4.html) was used.
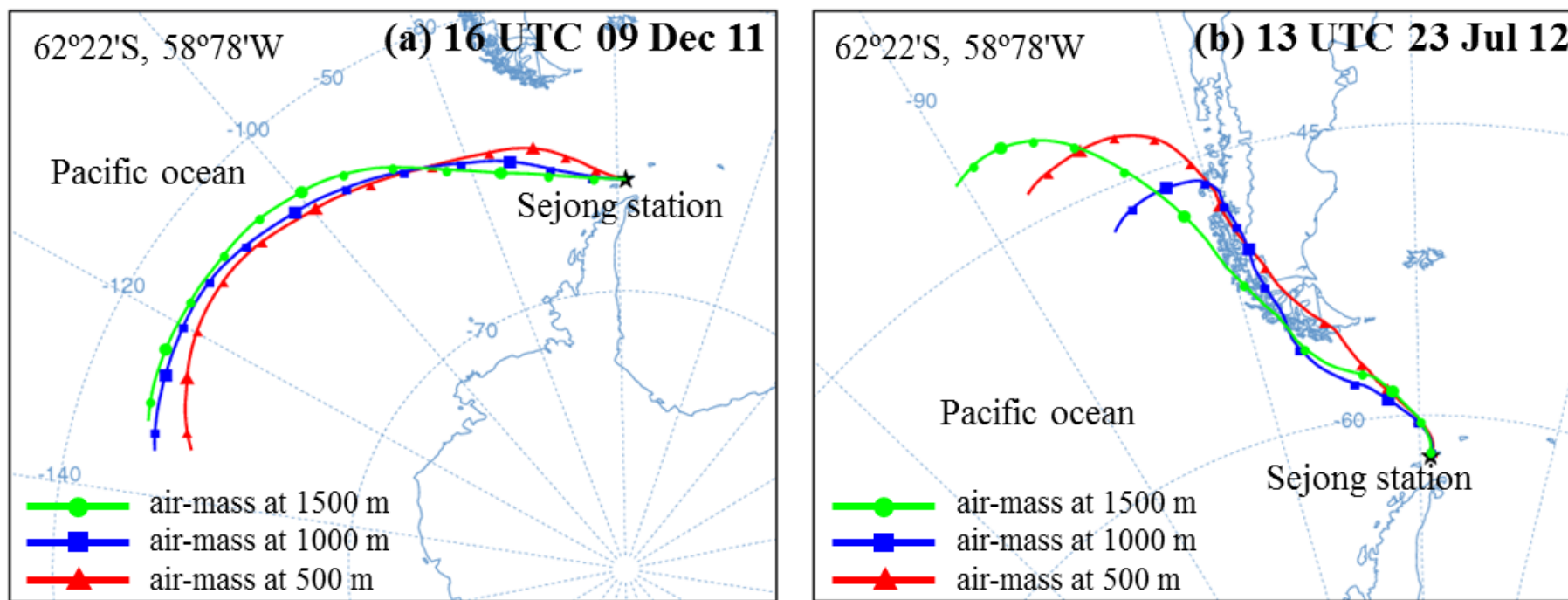
Figure S2. Relative abundances of individual particles in two size fractions of the summer and winter samples, having specific concentration ratios of (a) C, (b) S, (c) Ca, (d) Cl, (e) Mg, and (f) K to Na. The red solid and dotted lines demote the stage 2 ($PM_{2.5-10}$) and stage 3 ($PM_{1.0-2.5}$) particles of the summertime sample, respectively, and the blue solid and dotted lines are for stage 2 ($PM_{2.5-10}$) and stage 3 ($PM_{1.0-2.5}$) particles of the wintertime sample, respectively. The green lines indicate bulk sea-water ratios corresponding to the elements.

Figure S3. Raman and ATR-FTIR spectra of the aerosols generated by the nebulization of a mixture solution of 0.2 M alanine and 0.1 M $MgCl_2$ standard chemicals. The first pair of Raman and ATR-FTIR spectra for the aerosols was obtained just after the nebulization and the second and third pairs of Raman and ATR-FTIR spectra were obtained ~1 year later after the storage in a desiccator. The first and third pairs of Raman and ATR-FTIR spectra for organic moiety look similar to those in Figures 4(b) and 4(a), respectively.

Figure S4. Raman and ATR-FTIR spectra of some target chemicals for organics in Antarctic SSAs, which do not resemble with those for MgAla-containing SSAs.
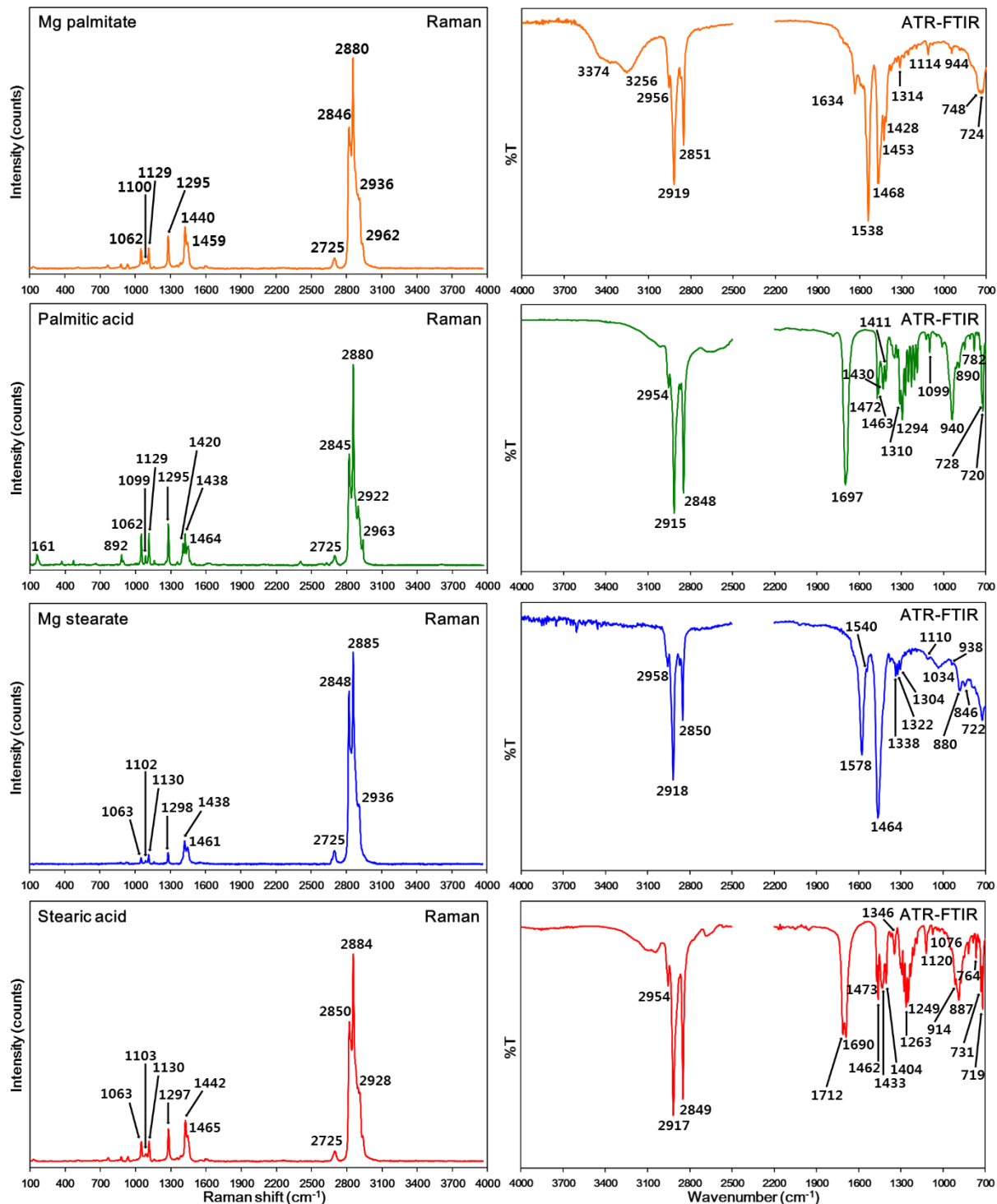
Figure S5.

39

Figure S6. <mark>ATR-FTIR spectra of Mg palmitate, Mg stearate, a mixture of Mg palmitate and stearate (by 3:1), and MgFAs-containing SSA, showing that MgFAs-containing SSAs are the mixture of mainly Mg palmitate and stearate.</mark>
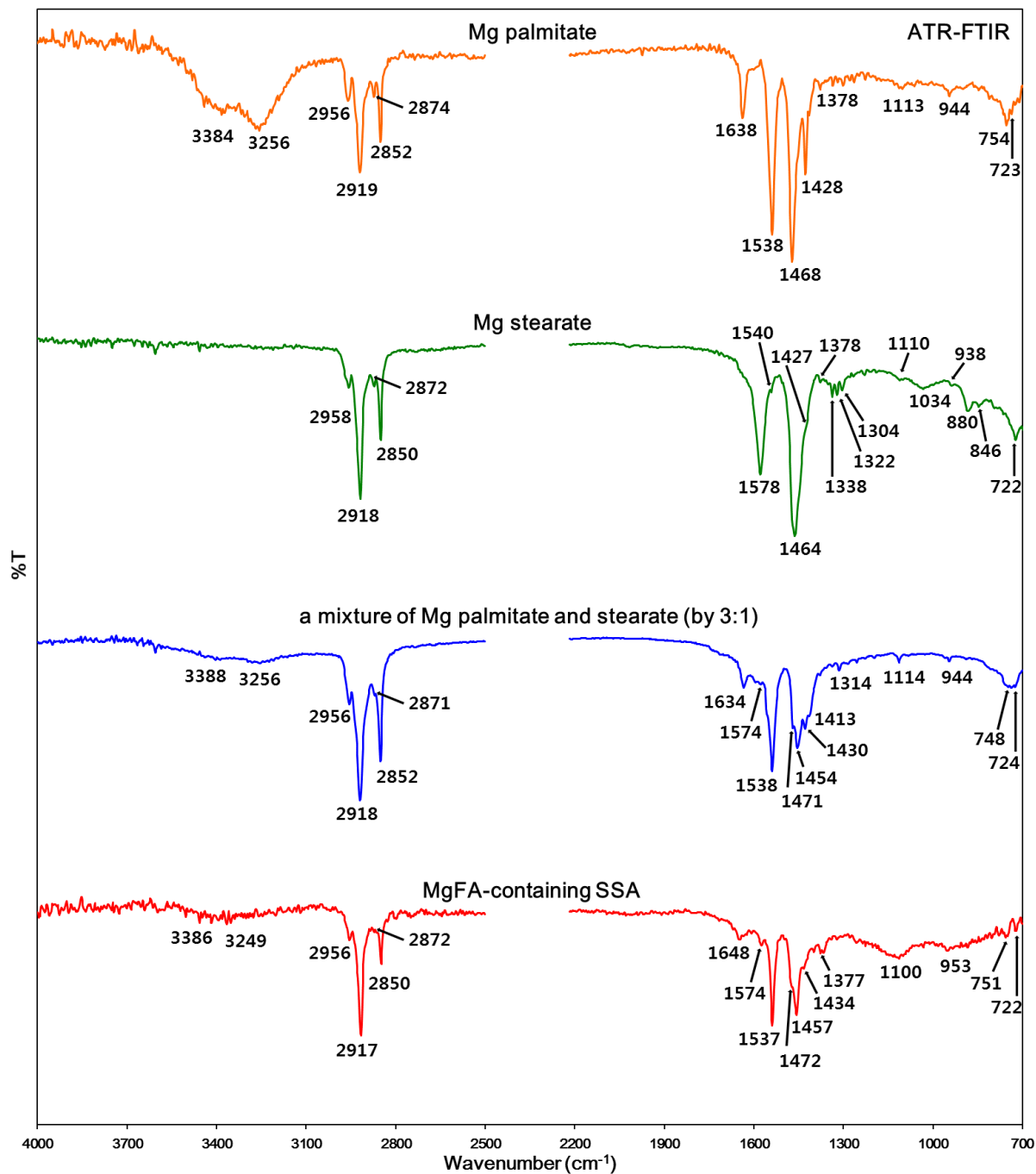
Figure S7. Raman and ATR-FTIR spectra of standard inorganic chemicals, which are observed in Antarctic SSAs.